A COMPARISON OF IONOSPHERIC MODEL PERFORMANCE FOR INTERNATIONAL SPACE STATION ORBITS

THESIS

David J. Broadwater, Captain, USAF

AFIT-ENP-13-M-04

DEPARTMENT OF THE AIR FORCE
AIR UNIVERSITY

AIR FORCE INSTITUTE OF TECHNOLOGY

Wright-Patterson Air Force Base, Ohio

AFIT-ENP-13-M-04

A COMPARISON OF IONOSPHERIC MODEL PERFORMANCE FOR INTERNATIONAL SPACE STATION ORBITS

THESIS

Presented to the Faculty

Department of Engineering Physics

Graduate School of Engineering and Management

Air Force Institute of Technology

Air University

Air Education and Training Command

in Partial Fulfillment of the Requirements for the

Degree of Master of Science in Applied Physics

David J. Broadwater, BS

Captain, USAF

March 2013

AFIT-ENP-13-M-04

A COMPARISON OF IONOSPHERIC MODEL PERFORMANCE FOR INTERNATIONAL SPACE STATION ORBITS

David J. Broadwater, BS
Captain, USAF

Approved:

Lt Col Ariel O. Acebal, PhD (Chairman)	7 MAR 13 Date
William F. Bailey, PhD (Member)	7 Mar '13 Date
Larry Gardner, PhD (Member)	3/8/2013 Date

AFIT-ENP-13-M-04

Abstract

Accurately modeling the ionosphere is crucial to forecasting potential operational impacts, including spacecraft charging, radio communication blackout, navigational errors, and safety issues for astronauts. The Floating Potential Measurement Unit (FPMU) aboard the International Space Station (ISS) monitors the ISS charging environment and provides a unique electron density and electron temperature in-situ data source just above the F_2 peak for the purpose of ionospheric model validation. Since FPMU data availability is limited, an ionospheric model that accurately predicts the ISS plasma environment is desirable for ISS mission planning and situational awareness when FPMU data is unavailable. Electron densities and temperatures from four ionospheric models (International Reference Ionosphere [IRI], Coupled Thermosphere Ionosphere Plasmasphere Electrodynamics model [CTIPe], Ionospheric Forecast Model [IFM], and Global Assimilation of Ionospheric Measurements model [GAIM]) were compared to in-situ FPMU values across a range of geomagnetic and solar conditions. The climatological and assimilative models (IRI and GAIM) performed the best overall across all conditions, while the pure physics based models (IFM and CTIPe) struggled the most to accurately predict the ISS plasma environment. The models struggled most during severe solar minimum conditions and periods of moderate geomagnetic and high solar activity. IRI-2012 and GAIM represent the best candidates for use by NASA as an ISS mission planning tool.

Acknowledgements

First, I would like to thank my wife for being so supportive of my school work for the last eighteen months. She put up with me spending long hours at AFIT and many late nights to complete this project. Your love and support fueled this effort.

Next, I would like to thank Lt Col Ariel Acebal for being such a great research advisor and mentor. None of this would have been possible without your motivation and guidance. Your operational focus and sense of humor helped make this process more worthwhile and enjoyable. Thanks for pushing me to put everything I have into this project and demanding excellence.

I would also like to thank Dr. William Bailey for giving me the foundation in plasma physics required to complete this research and for being a member of my thesis committee. Thanks for being so supportive of my research and for making sure I'm well prepared to discuss plasma physics at cocktail parties should the need arise.

Likewise I would like to thank Dr. Larry Gardner for being a member of my committee and his help in running the models. Thanks for taking the time to teach me how the models worked, for always answering my questions, and for helping me troubleshoot when the need arose. Your hospitality (as well as that of the whole Utah State University SWC team) is sincerely appreciated.

I would like to thank the folks at NASA MSFC for providing the data used in this effort and for explaining the ins and outs of the FPMU and I'd like to thank NASA CCMC for providing assistance in running some of the models used in this effort.

Lastly, I would like to thank my family for always encouraging and supporting me in all my endeavors, academic or otherwise.

Table of Contents

Page

Page

List of Figures

List of Tables

Table Page

A COMPARISON OF IONOSPHERIC MODEL PERFORMANCE FOR INTERNATIONAL SPACE STATION ORBITS

I. Introduction

1.1 Motivation and Background

As our reliance on satellites, Global Positioning System (GPS) navigation, and long range communication increases, it has become critical to better understand the environment our satellites and radio signals operate in and through, known as the ionosphere. The ionosphere is the near earth subset of space located roughly between 90 km and 1500km and its conditions can fluctuate depending on geomagnetic storming conditions, time of day, seasons, solar cycle, and solar activity. These events can cause radio communication blackout, navigational errors, spacecraft charging, safety issues for humans in space, and other hazards. Accurate ionospheric modeling is crucial to help mitigate and predict these threats.

1.2 Impact of the Ionosphere on the International Space Station

The International Space Station (ISS) operates at an altitude of 400km, above the peak plasma density height of the ionosphere(typically around 300km); the area above this peak is known as the topside ionosphere. The ISS has many missions, some of which involve Extra Vehicular Activities (EVAs), or spacewalks, to perform repairs to the ISS and/or experiments. Due to safety concerns from charging, NASA has identified a risk to astronauts during EVAs if the ISS charges to more than 40 volts (*Ferguson et al.*, 2003). Charging of the ISS can be especially significant when

it passes through areas of cold, high-density plasma; this can lead to high potential differences between the ISS and the surrounding plasma and lead to arcing.

The ISS measures the surrounding ionosphere with an instrument called the Floating Potential Measurement Unit (FPMU). The FPMU was installed because the ISS faces unique charging situations; not only do astronauts on board need to perform EVAs, but also the ISS solar panels are much larger and operate at a much higher voltage than most spacecraft (*Carruth et al.*, 2001). The exposed interconnects between the solar panels can accumulate ions as the ISS travels through the ionosphere, creating an electrical potential difference with the surrounding plasma (known as floating potential), causing charging. While one of the functions of the FPMU is to measure the surrounding ionosphere to try to understand why the ISS charges, its primary purpose is to monitor charging levels of the ISS and provide data that can be used to validate the ISS charging models (*Barjatya et al.*, 2009). As a result, the FPMU is not operated continuously; it is activated by commands from the ground and only records data for specific time durations when ISS charge monitoring is deemed most necessary (i.e., prior to an EVA, during an ISS configuration change, etc.).

1.3 Ionospheric Modeling

Various computer-based models have been created to help predict densities and temperatures throughout the ionosphere. Many validation efforts for these models have taken place below the peak plasma density of the ionosphere due to the ability of using ionosondes to determine plasma densities at various altitudes (*Tascione*, 2010). Similarly, total electron content (TEC) measurements have been taken using signals from various satellites (mostly GPS) that travel through the ionosphere. However, limited work has been done to validate these models for the topside ionosphere due to the difficulty in obtaining plasma density data in that region, since radio signals

either pass through the ionosphere or are reflected before they reach the peak plasma density. While signals that pass through the ionosphere enable the calculation of TEC values, reflected signals are critical to determining electron density values at specific heights, since reflection is driven by the plasma frequency in a certain region, which is directly related to electron density. The heights associated with those density values are determined by the time it takes for a signal to be reflected back. As a result, most models use plasma density values from the bottom-side ionosphere, TEC values, and electron transport models to extrapolate plasma densities for the topside ionosphere (*Reinisch and Huang*, 2001).

1.4 Research Focus

This research effort aims to answer two main questions: How well do the current ionospheric models perform in the topside ionosphere just above the F_2 peak? Are the current ionospheric models accurate enough at ISS orbits for NASA to use them for mission planning and to predict electron densities and temperatures when the FPMU is unable to collect data?

1.5 Document Organization

The remainder of this document is organized as follows: in Chapter II, theory related to the ionosphere is explained, along with a brief description of each of the ionospheric models used in this effort. Chapter III describes the research methodology used in this effort. Next, analysis results are presented in Chapter IV. Finally, a summary of the results and recommendations for future work are given in Chapter V.

II. Background

This chapter provides background information about the ionosphere, the ionospheric models considered in this effort, and the data source on the International Space Station used for validation.

2.1 The Ionosphere

The ionosphere is the region of Earth's atmosphere located from 90 km to 1500 km above Earth that contains a large amount of ions and electrons formed primarily from photoionization from extreme ultraviolet and soft x-ray radiation from the Sun. These ions and electrons are subject to many different processes, including chemical reactions, diffusion, recombination, and transport by neutral winds. The ions and electrons form a plasma, which is a population of ionized (e.g., charged) particles that are quasi-neutral as a whole and exhibit collective behavior. This plasma is very important because it can create charging hazards for spacecraft and affect signal propagation through the ionosphere, potentially affecting all satellite and certain radio communications.

The main source of ionization in the ionosphere is photoionization caused by solar radiation. While solar irradiance increases with altitude, densities of the neutral particles that become ionized by this solar radiation decrease with height; this creates a peak in ionization known as a Chapman layer (Figure 1). Chapman layers, combined with chemical ion/electron production and loss processes, diffusion, and transport mechanisms, create several distinct layers (D, E, and F) in the ionosphere, with different processes dominating in each layer. Chemical processes dominate in the D (60-100 km) and E (100-150 km) regions, where neutral densities are greater. Typical ion/electron densities in these regions are on the order of $10^{11}\ m^{-3}$. Transport

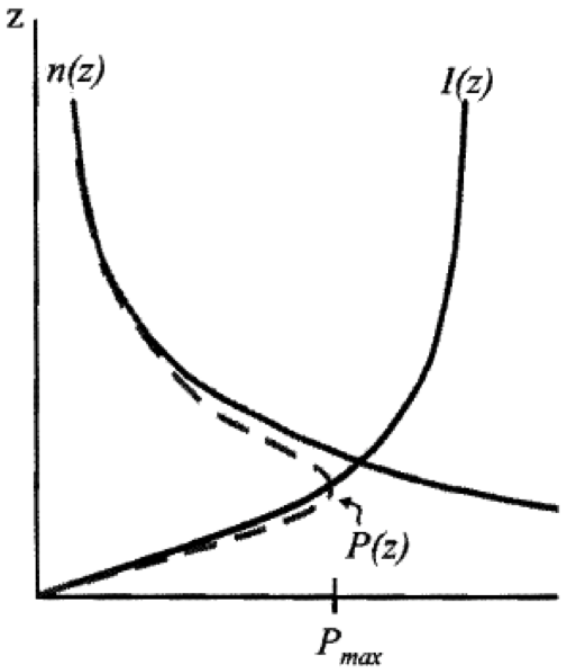

Figure 1. Chapman layer and ionization curve (dashed line). (Adapted from *Steadman* 2011)

processes have a larger impact in the F region, which is split further into two regions: F_1 (150-250km) and F_2 (250-600km). These transport processes lead to larger electron densities, and increase until they reach the F_2 region, where the transport processes dominate. A distinct peak is formed in the F_2 region where the plasma transport mechanisms balance the chemical loss processes, typically on the order of 10^{12} m^{-3} (*Schunk and Nagy*, 2009). The region above the F_2 peak is generally known as the topside ionosphere. Figure 2 shows a vertical profile of the distinct layers.

Typical ionospheric parameters include electron density (N_e), ion density (N_i), electron temperature (T_e), total electron content (TEC), density of the F_2 peak (NmF_2), and the height of the F_2 peak (hmF_2). TEC is the total integrated number of electrons between two points, usually measured vertically. It is one of the most common parameters used for the comparison of ionospheric models due to the ability of GPS satellites to measure TEC from distortions in transmitted signals. Due to

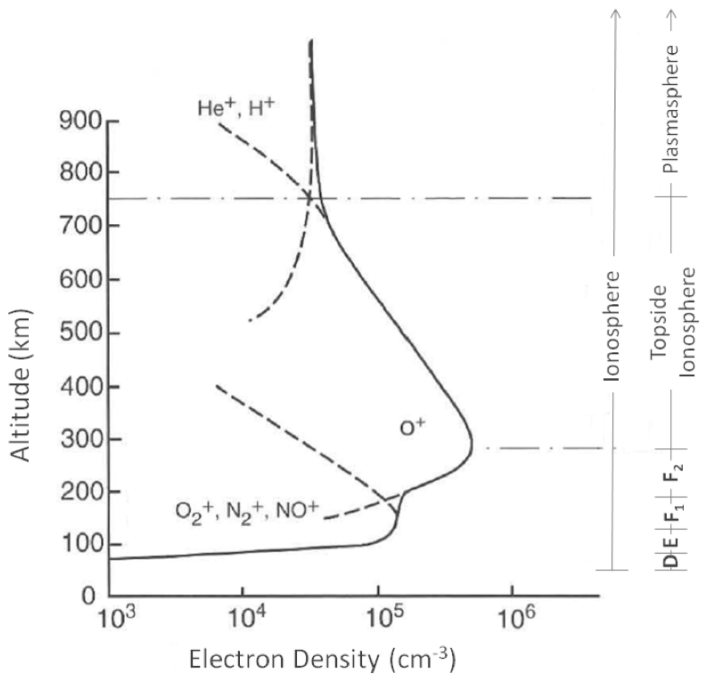

Figure 2. Vertical profile of the ionosphere. (Adapted from *Banks et al.*, 1976)

the sensors incorporated into the FPMU, this effort will focus on electron density and electron temperature. Model-predicted TEC will also be considered as a means to further compare model differences among electron densities and observe overall trends.

2.1.1 Electron Density Anomalies.

While there are many different electron density anomalies, two of the most common are the Appleton Anomaly and plasma bubbles. The Appleton anomaly occurs in equatorial regions during the daytime. It is caused by eastward ionospheric currents generated by the neutral wind that drive an upward plasma flow, which then diffuses down magnetic field lines due to gravity. It creates a fountain-like effect, with enhancement in plasma densities on either side of the magnetic equator (*Schunk and Nagy*, 2009). Plasma bubbles occur primarily at night, also near the magnetic equator and partially due to the same processes that create the Appleton anomaly. Around

dusk, there is an enhancement in the eastward electric field from increased neutral winds at dusk and conductivity gradients across the terminator, sometimes known as pre-reversal enhancement. This increased electric field again drives an upward plasma flow; however, the local ionosphere then rotates into the night sector, where production from sunlight ceases and chemical loss processes dominate, causing a swift decrease in electron densities in the F_1 layer. This in turn creates what is known as a Rayleigh-Taylor instability, where a high-density fluid is above a low density fluid. Once a perturbation in the boundary layer is created (sometimes by gravity waves), magnetic field-aligned electron density depletions can then grow rapidly into plasma bubbles. They can reach heights of 1500 km, grow as quickly as 5 km s^{-1}, and extend horizontally for several thousand kilometers (*Schunk and Nagy*, 2009).

2.1.2 Electron Temperature.

The electron temperature is an indication of how much energy is present in a plasma. The electron energy is important because it determines what kinds of collisions and reactions can take place, which drive the creation of ions, electrons, and the ionosphere in general. Additionally, electron density and electron temperature tend to be inversely correlated, because electron cooling rates are higher when electron densities are greater (*Schunk and Nagy*, 2009).

2.2 Ionospheric Models

While many different models exist for the ionosphere, four will be considered in this effort, with multiple versions of certain models compared in some cases: International Reference Ionosphere (IRI), Coupled Thermosphere Ionosphere Plasmasphere Electrodynamics (CTIPe), Ionospheric Forecast Model (IFM), and Global Assimilation of Ionospheric Measurements (GAIM). Each model takes a different approach

to modeling the ionosphere and is well established, providing a good sample set of ionospheric models against which FPMU data is compared. The GAIM model holds special interest from an Air Force perspective, since it is used operationally by the Air Force Weather Agency to help predict the operational impact of conditions in the ionosphere.

Each ionospheric model is briefly described here, since a detailed description of each would be impractical for this effort. Descriptions includes model inputs, outputs, and availability, as well as references for more in-depth information about each model for the reader.

2.2.1 International Reference Ionosphere.

IRI (International Reference Ionosphere) is an empirical computer-based ionospheric model sponsored by the Committee on Space Research (COSPAR) and the International Union of Radio Science (URSI). It is based on a wide range of ground and space data from a worldwide network of ionosondes, as well as in situ instruments on many satellites and rockets (*Bilitza and Reinisch*, 2008). Because many of these data sources are at mid-latitudes, it tends to perform better there than at low latitudes(*Bilitza et al.*, 2011). IRI is considered the international standard for the ionosphere by the International Organization for Standardization (ISO).

Since IRI is an empirical model, it is updated regularly as new measurement data emerges and provides a climatological reference to compare to forecasts from other models. IRI-90 was the first version of the IRI model to be released as a computer model. IRI-2012 is the most recent version of the IRI model. Since it was released recently, there are very few studies that have used the model. However, IRI-2007 (the major version prior to IRI-12) has been used extensively. IRI-12 includes a new NmF_2model and topside electron density model, along with updated averages (*Bilitza*

et al., 2011).

Required inputs for IRI-1990 and IRI-2012 include latitude, longitude, height, 3-hour Ap magnetic index, as well as daily, 365-day averaged, and 810-day averaged F10.7 index values. IRI outputs include electron temperature, electron density, ion drift, ion composition (O^+, H^+, N^+, He^+, O_2^+, NO^+, and $Cluster^+$), and ion temperature, all from 50-1500km (*Bilitza and Reinisch*, 2008). IRI is the only model compared in this effort that does not produce three-dimensional output. All major versions of IRI (including those used in this effort) are available for download as FORTRAN code at http://iri.gsfc.nasa.gov/.

2.2.2 Coupled Thermosphere Ionosphere Plasmasphere Electrodynamics Model.

The Coupled Thermosphere Ionosphere Plasmasphere Electrodynamics (CTIPe) model is a global, three-dimensional, time-dependent physics-based model that incorporates models of four distinct components (*Codrescu et al.*, 2012) These include a global thermosphere model, a high-latitude ionosphere model, a mid- and low-latitude ionosphere/plasmasphere model, and an electrodynamical calculation of the global dynamo electric field. The CTIPe model runs each of these components concurrently and couples them with respect to energy, momentum, and continuity (*Codrescu et al.*, 2012). The CTIPe model is currently used by NOAA's Space Weather Prediction Center to model the ionosphere. Additionally, CTIPe can be run online through NASA's Community Coordinated Modeling Center (CCMC) at http://ccmc.gsfc.nasa.gov/models/modelinfo.php?model=CTIPe.

Required inputs include F10.7 index values (daily F10.7 and 90-day average F10.7), magnitude of the magnetic field, IMF clock angle, dipole tilt, solar wind speed, solar wind density, Hemispheric Power index value, and Hemispheric power in gigawatts.

CTIPe has a 2° latitude resolution, an 18° longitude resolution, with vertical spacing broken up into 15 pressure levels at a resolution of one scale height. Outputs include neutral densities of O_2, O and N_2, electron densities, and ion densities (O^+, H^+, N^+, O_2^+, N_2^+) from 140km to 2000km. CTIPe can also calculate ion and electron temperatures, but only within geomagnetic latitudes of ± 50°.

2.2.3 Ionospheric Forecast Model.

The Ionospheric Forecast Model (IFM) is a physics-based numerical solution of the global ionosphere using plasma continuity, momentum and energy equations (*Zhu et al.*, 2006). It was developed by Utah State University (USU) and can provide a 24-hour forecast of the ionosphere in 30 minute increments. The number of inputs required for IFM is actually less than IRI; IFM only requires the date, run duration, F10.7 index values, and Kp index values. It creates a three-dimensional, time-dependent density distribution of electrons and the major ion constituents (H+, O+, NO+, and O2+) in the ionosphere, as well as electron and ion temperatures. IFM's 3-D grid has a resolution of 3° latitude and 7° longitude. Vertically, output spans from 90-1600km, and vertical resolution is 4km in the E region and 20 km in the F region (*Scherliess et al.*, 2006). IFM calculates electron temperatures using two different models (*Schunk*, 2012). Within ± 45° of the geomagnetic equator, Titheridge's empirical electron temperature model is used (*Titheridge*, 1998). Above ± 20° geomagnetic latitudes, electron temperature is calculated from a numerical solution to the continuity, momentum, and energy equation (*Schunk et al.*, 1986). Then, the electron temperature values from both models are blended from ± 25° to ± 40° magnetic latitude. Electron temperature values are then used by IFM to calculate electron density values.

2.2.4 Global Assimilation of Ionospheric Measurements Gauss-Markov Model.

The GAIM-GM model is a time dependent physics-based model that uses the Ionospheric Forecast Model (IFM) as a background model upon which perturbations are imposed via a Kalman filter data assimilation scheme. Various data types can be imported, including in situ electron densities and line of sight TEC values from satellites. The GAIM model was also developed by Utah State University and is currently used by the Air Force Weather Agency for ionospheric modeling. GAIM determines the best selection of data sources (for a given combination of overall data sources; i.e., GPC TEC values) and applies known biases and weights to the assimilated data. Assimilated data deemed too different from the IFM is discarded as bad data. Then, the remaining values are superimposed onto the IFM background using a sequential least squares fit. GAIM requires numerous inputs due to the fact it is an assimilative model; it can assimilate bottom-side electron density profiles from ionosondes, slant and vertical TEC from GPS stations, DMSP in-situ electron densities, and line of sight UV emissions measured by DMSP (*Scherliess et al.*, 2006). The overall GAIM workflow is shown in Figure 3.

Like IFM, GAIM output is also in the form of a 3-D grid. However, GAIM only assimilates and produces values related to electron densities. Outputs include NmE, hmE, NmF_2, hmF_2, electron densities, and slant and vertical TEC values. GAIM has a resolution of 4.67° latitude and 15° longitude, the coarsest resolution of any of the models considered in this effort. A regional mode is available with a resolution of 1° latitude and 3.75° longitude, but only after GAIM has been run globally. Lastly, GAIM can be run in a forecast mode up to 24 hours out. GAIM is available online at http://ccmc.gsfc.nasa.gov/models/modelinfo.php?model=USU-GAIM.

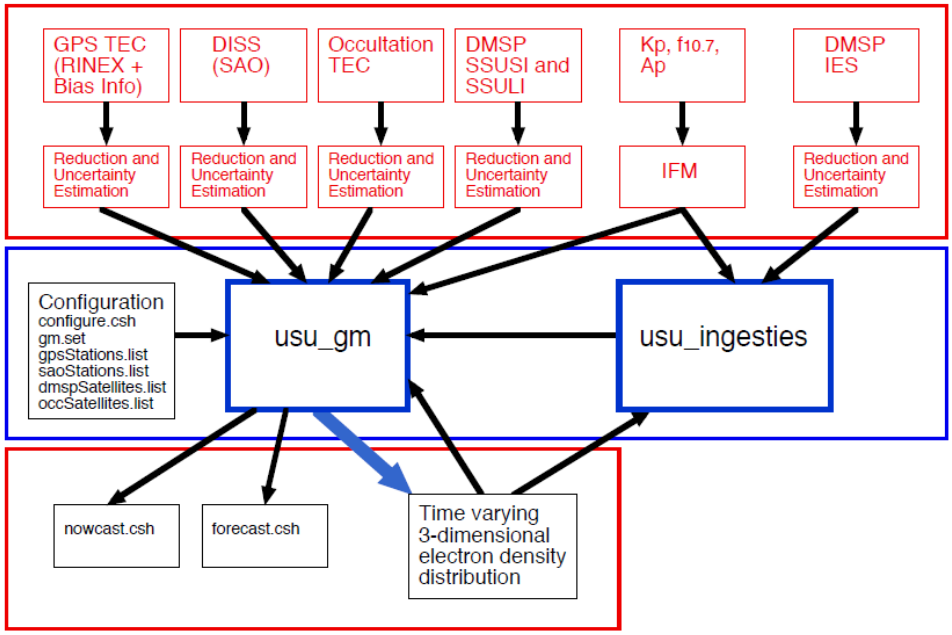

Figure 3. GAIM-GM model run flowchart depicting how data is assimilated into the model.

2.3 Electron Density and Electron Temperature and the ISS

The ISS is an ideal candidate for testing the validity of the ionospheric models because of its short orbital period (91 minutes), orbital inclination (51.7°), and location in the ionosphere. Its short orbital period allows for many orbits worth of data to be analyzed for a given day across different seasons and locations. The ISS also provides a unique in-situ data source for electron density and electron temperature data just above the F_2 peak.

The ISS faces unique manned spacecraft charging hazards due to the high voltage of its solar arrays (*Ferguson et al.*, 2003). It has been determined that a potential difference of 40V or greater represents a hazard to astronauts during EVAs, and that the largest potential differences occur when the ISS is traveling through a region of cold, high-density plasma.

To mitigate this hazard, two plasma contactor units are powered on for the duration of all EVAs and replenishes the electrons collected by the high-voltage solar

arrays, reducing the potential differences to safe levels. While the plasma contactor units completely mitigate these charging hazards, a secondary hazard mitigation plan must be in place in case one of the plasma contactor units fails. In order to monitor the charging environment on the ISS, NASA installed the Floating Potential Measurement Unit (FPMU) on the ISS in 2006. The FPMU was created by Utah State University's Space Dynamics Laboratory and was installed on the ISS in 2006.

2.4 Floating Potential Measurement Unit

The floating potential measurement unit (FPMU), shown in Figure 5, was designed to be capable of providing redundant measurements of various plasma parameters and consists of four probes: a Floating Potential Probe (FPP), a Wide-Sweeping Langmuir Probe (WLP), a Narrow-Sweeping Langmuir Probe (NLP), and a Plasma Impedance Probe (PIP). The FPP measures the ISS floating potential (the potential difference between the ISS and the surrounding plasma), while the WLP and NLP measure the ISS floating potential, the electron density, and the electron temperature. The values measured by the WLP and NLP have been shown to agree within 10% (*Barjatya et al.*, 2009).

Electron densities and temperatures are computed by measuring the current resulting from a range of applied voltages, and then applying a complicated fitting process to the resulting data to derive electron densities and temperatures (*Wright et al.*, 2008). This is sometimes known as a "graphical method" and each region of the resulting current-voltage (or I-V) plot is treated separately. The three main regions in the I-V curves are the ion saturation region (where the net ion current dominates), electron retarding region (where the ion current is negligible, but there is enough of a negative potential to partially repel electrons), and the electron saturation region (where the net electron current dominates). An example of a typical I-V curve from

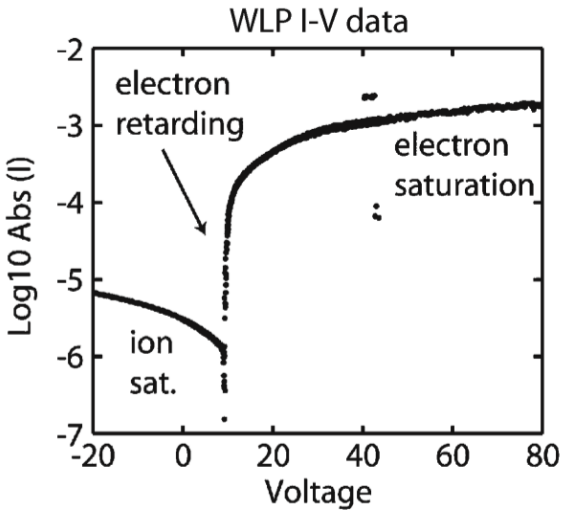

Figure 4. A sample I-V curve created by a current-voltage sweep performed by the FPMU WLP. Note the three distinct regions in the plot. The voltage at which the current changes polarity (9.2 V) is the potential of the ISS. This plot follows the "Langmuir Convention," with ion current recorded as negative and electron current as positive (Adapted from *Wright et al.* 2008).

this analysis is shown in Figure 4.

There are many steps involved in deriving electron densities and temperatures from the raw FPMU data, which will be summarized here. A more thorough treatment is provided in *Wright et al.* (2008). First, the applied voltage that causes a change in current polarity is found and assumed to be the measured potential of the ISS (i.e., the floating potential). This change in polarity defines the boundary between the ion saturation region and the electron retarding region of the I-V curve. Then, a correction is applied to the current values to account for the photoelectron current. A least squares fit is then applied to the ion saturation region (assuming a linear relationship between ion current and the applied voltage) to determine the ion current baseline, which can then be subtracted from the measured current to determine the electron current. Finally, the voltage of the surrounding plasma is determined by finding the voltage corresponding to the maximum value of the first derivative of the electron current.

The calculated ion current is then assumed to be equivalent to the ion ram current

(I_{ram}), since the ISS orbits at a speed greater than the ion thermal speed (but below the electron thermal speed). Since the ISS is moving faster than the ion thermal speed, it is assumed that ions collected by the ISS are not dependent on the temperature of the ions. By making this assumption, the ion density can be calculated by using the relation

$$I_{ram} = q \cdot N_i \cdot V_{ISS} \cdot A_{LP} \tag{1}$$

where q is the electronic charge, N_i is the ion density, V_{ISS} is the magnitude of the ISS velocity, and A_{LP} is the cross sectional area of the Langmuir probe. For this study, the spherical WLP was used for calculating ion densities, so the cross section was constant. The electron density values provided by NASA for this effort were actually derived ion densities. Comparisons of WLP and NLP electron and ion densities to COSMIC satellite in-situ electron densities have shown the WLP ion densities to correlate much better to the COSMIC electron densities than the electron densities from either probe, with the electron densities generally significantly less than the derived ion densities (*Gurgew*, 2011). Since the ionosphere is a quasi-neutral plasma, the ion and electron densities should theoretically be the same. NASA believes this discrepancy is due to the differences in deriving electron and ion densities from the raw data (*Gurgew*, 2011). Due to these issues, NASA has decided to report the derived ion densities as electron densities (*Minow*, 2012).

Electron temperatures are then calculated using the derived electron current and potential of the surrounding plasma (plasma space potential). It is assumed that the electrons in the electron retarding region are Maxwellian and follow a Boltzmann relation for electron current (I_e) given by

$$I_e = I_{eo} \cdot \exp\left[\frac{q(V - V_{sp})}{kT_e}\right] \tag{2}$$

where q is the electron charge, k is Boltzmann's constant, V_{sp} is the plasma space potential, T_e is the electron temperature, and I_{eo} is the random electron thermal current and is given by

$$I_{eo} = \frac{q \cdot N_e \cdot A_p}{4} \cdot \left(\frac{8kT_e}{\pi m_e} \right)^{1/2} \tag{3}$$

where N_e is the electron density, A_p is the area of the Langmuir probe, and m_e is the electron mass. These relations are then used in the curve fitting process in the electron retardation region to determine the electron temperature values. Average fit errors are calculated only for electron temperatures, and are generally less than 1%, while variations in the electron density and temperature data suggest errors closer to 10% for both, although a detailed error analysis has yet to be performed (*Minow*, 2012). While not used in this effort, electron densities are derived from the I-V curve data by substituting the derived electron temperature value and potential of the surrounding plasma into Equation 3 and solving for electron temperature.

While electron temperatures and densities measured by the WLP and NLP have been shown the be within 10% of one another, it is difficult to validate the values themselves due to the lack of in-situ electron density data at ISS altitudes. A limited validation effort was performed by *Coffey et al.* (2008) by comparing FPMU measured data to electron densities measured by the TIMED-SEE satellite, ionosondes, and an incoherent scattered radar (ISR) site within a certain temporal and spatial range relative to the ISS. Then, IRI-2007 was used to determine the average expected ratio between the FPMU values and the other values (all at different altitudes than the ISS), and relative differences were calculated to to see how often the percent difference between the two sets of values were within the expected ratios. The TIMED-SEE values were within the accepted difference value 28% of the time, while ionosonde data differences were within the expected value 74% of the time and ISR differences

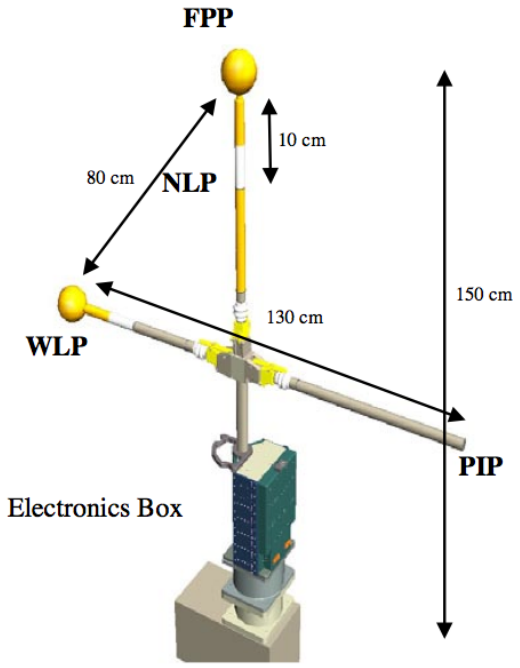

Figure 5. FPMU Diagram (Adapted from *Gurgew* 2011)

were within the expected value 66% of the time. Electron temperature values were compared in the same manner for the ISR site, and the differences were within the expected value 26% of the time. It is believed that the conjunctive comparison process played a significant role in the larger observed differences than expected.

To provide a backup charging hazard mitigation plan for an EVA, NASA collects FPMU electron densities for 2-3 days prior to a scheduled EVA. Then, it also produces IRI-2007 model output for the same period using ISS ephemeris data and determines how well the FPMU data is correlating to IRI output. Then, NASA determines if the FPMU data correlates more strongly with unchanged IRI output, or if an offset applied to the IRI output provides a better fit. Then, the "corrected" (if necessary) IRI data is input into a computer model called the Plasma Interaction Model (PIM) which simulates ISS charging conditions based on various ISS electrical configurations. The PIM output indicates whether any steps need to be taken to alter the electrical current path of any of the solar panels to reduce the charging hazard, or if the standard

charging configuration is safe based on the ionospheric conditions from the IRI-2007 output (*Minow et al.*, 2002).

During initial efforts to determine the charging effects and levels the ISS would experience, it was discovered that more electrons would be collected by the ISS solar arrays for lower electron temperature values than for higher ones. This is contrary to the assumed relation where a conductor with a positive bias should collect an electron current proportional to the electron density and to the square root of the electron temperature (i.e., the thermal current density). Due to the fact that only the edges of the solar cells are exposed to the plasma and are partially "hidden" from the plasma due to construction and spacing of the cells, a potential barrier is created that "preferentially excludes high-temperature electrons and admits low-temperature electrons" (*Ferguson*, 2009). By analyzing electron temperature and density data near peak charging times (generally eclipse exit) measured by a device called the Floating Potential Probe (FPP), which was the predecessor to the FPMU on the ISS and performed a similar function, the Ferguson-Morton relation was established and is given by

$$\Phi = -2.6907\ N_e^{0.1057}\ \exp(-8.02\ T_e) \tag{4}$$

where Φ is the charging potential (V), N_e is the electron density ($\#/m^3$), and T_e is the electron temperature (eV). While this relation was originally calculated when the ISS only had two solar arrays (it currently has four), the same general relation is expected to hold, while the specific coefficients themselves may be different in the current configuration (*Minow*, 2012). From Equation 4 we see that small changes in electron temperatures can cause large charging potentials. Due to the general inverse relationship between electron density and temperature near the F_2 peak, some of the lowest electron temperature values are associated with high electron densities, com-

pounding the charging effect. While charging due to magnetic induction provides a significant contribution to the ISS charging levels, it is not dependent on the densities and temperatures of the surrounding plasma. The largest observed potential differences tend to occur during eclipse exit (the times for which Equation 4 are assumed to be valid) and are dependent on the electron temperatures and densities, due to the fact that the solar arrays operate at a positive voltage which acts to attract electrons and drive the ISS potential more negative (*Wright et al.*, 2008).

2.5 Previous Efforts

A limited set of FPMU ion densities were compared to the IRI and GAIM models by (*Barjatya et al.*, 2009) in 2009, and while they did not provide quantitative data regarding the differences between the data, both models were in general agreement with the in-situ measurements, with GAIM tracking the FPMU values better. Their results show that in situ density measurements agree better with the GAIM model than the IRI model in general, which is expected due to GAIMs data assimilative nature. Temperatures were only compared to the IRI model, but also were said to be similar to the in situ values.

III. Methodology

3.1 Representative Ionospheric Conditions

In order to thoroughly test the validity of the models, a wide range of ionospheric conditions were considered for this effort. Solar activity and geomagnetic storms have a significant impact on ionospheric conditions, so representative solar and geomagnetic activity conditions were used to compare the performance of these models. Geomagnetic storming conditions are given by the Kp index, which is a global index that measures the amount of variation in the horizontal magnetic field measured at earth and varies from 0-9. Solar activity levels are given by the F10.7 index, which measures the daily observed flux from the sun at a wavelength of 10.7 cm in solar flux units ($sfu = 10^{-22}\ W\ m^{-2}\ s$). Three time periods were evaluated during low solar activity (solar minimum): geomagnetic quiet conditions, moderate geomagnetic storming, and strong geomagnetic storming. Similarly, the same three geomagnetic conditions were evaluated during periods of moderate/high solar activity (solar maximum), for a total of six cases. Only time periods with at least five consecutive days of FPMU data were chosen for this study in order to provide an adequate sample size for each period and to examine the performance of the models during onset or recovery periods. Table 1 shows all of the dates selected, along with the maximum Kp and F10.7 value for the period.

3.2 Floating Potential Measurement Unit Data

All data from the FPMU is transmitted through the Ku frequency band, which is the high-bandwidth (video) communications band for the ISS. However, data or video from other ISS activities often take precedent over FPMU data transmission, resulting in gaps in FPMU data. Additionally, all of the Ku-band data is relayed through the

Table 1. Periods of study chosen for this effort and their associated geomagnetic and solar activity levels.

Run	Day of Year	Dates	Year	Geomagnetic Activity (Kp)	Solar Activity (F10.7)
1	253-256	10-13 Sept	2007	Quiet (1)	Quiet (67)
2	70-74	10-14 March	2008	Moderate (4)	Quiet (68)
3	95-99	5-9 April	2010	Storming (7-)	Quiet (78)
4	60-64	1-5 March	2011	Moderate (5+)	Active (130)
5	120-125	30 Apr - 5 May	2011	Moderate (5-)	Moderate (110)
6	292-296	19-23 October	2011	Quiet (2+)	Active (164)

Tracking and Data Relay Satellite System (TDRSS) to stations on the ground in the US; due to TDRSS communications limitations over Asia, no Ku-band data can be transmitted when the ISS is at $40-90^{\circ}$ longitude (*Minow*, 2012). However, due to the short orbital period of the ISS, it is still possible to obtain data from a representative range of latitudes at various local times. An example of ISS orbital data coverage is provided in Figure 6.

NASA provided the FPMU data in text file format. Each text file output included the year, decimal day of year (DOY), latitude (geographic), longitude, altitude, electron density ($\#/m^3$), electron temperature, and orientation of the ISS (pitch in degrees) on each line. Missing electron density or electron temperature values were identified with a value of -1. NASA used the WLP for electron density values, while they used the NLP for the electron temperature values; these were chosen because they had been determined to be the most accurate FPMU sensors for each respective parameter.

3.3 Running the Models

Each of the ionospheric models compared in this study is operated very differently. Unsurprisingly, the climatological models (IRI) required the least amount of effort and information to run, while the physics-based models required slightly more work

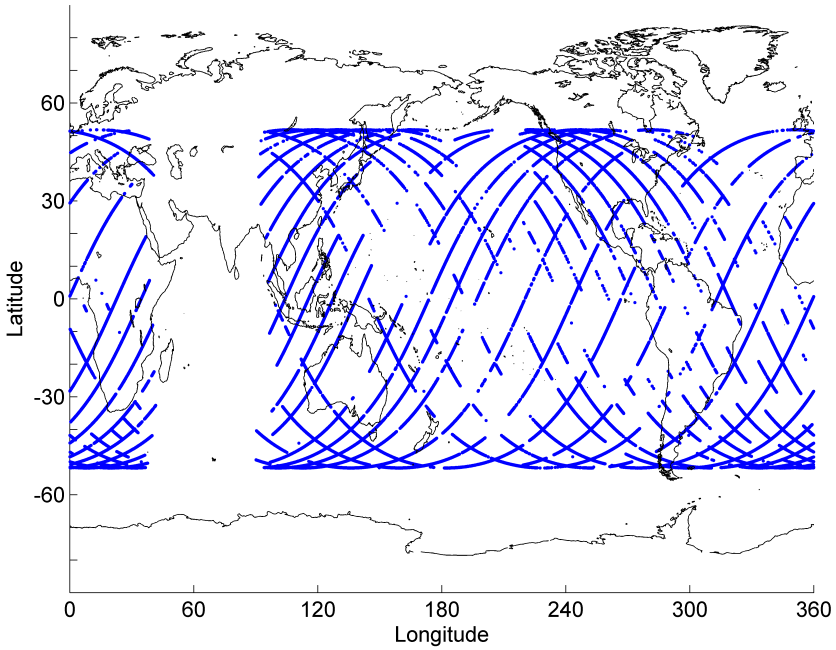

Figure 6. FPMU data coverage for 10-12 September 2007. Note the zone of exclusion (lack of data points) over $40 - 90^{\circ}$ longitude.

to run, and the data assimilation model required the most effort to run due to the need to download and prepare data for assimilation into the model. The processes required to operate each of the models are described below.

3.3.1 IRI 1990 and IRI 2012.

IRI-90 and IRI-12 were both run using FORTRAN codes (one for each of the two models) to ingest ISS times, locations, and heights into IRI-90 and IRI-12 to determine each models predicted electron density, electron temperature, and total electron content at each point in space and time where FPMU data existed. Total electron content values were calculated by integrating IRI predicted electron density values at each FPMU latitude and longitude from the surface of the earth to 1000 km in 10 km steps. NmF_2 and hmF_2 values were determined by finding the peak electron density value at each of those 10 km steps and the height at which that peak

value was found. Input flags used for both models are provided in Appendix A. Since these models do not run in a three-dimensional mode like the rest of the models, the output values were valid for the input ISS location and no interpolation of model results was required.

The output text files included year, decimal DOY (UT), latitude, longitude, altitude, FPMU-measured electron density ($\#/m^3$), IRI-predicted electron density ($\#/m^3$), FPMU-measured electron temperature (Kelvin), IRI-predicted electron temperature (Kelvin), local time (decimal hours), ISS orientation (degrees), and IRI-predicted TEC, NmF_2, and hmF_2 values on each line.

3.3.2 CTIPe.

All of the CTIPe runs completed for this effort were completed by using NASA's Community Coordinated Modeling Center (CCMC). Due to the unavailability of quality-controlled and hourly-averaged ACE data for some of the run periods for input into CTIPe, the CCMC ran all six runs using real-time ACE data for consistency amongst all runs. This also represents more of a realistic set of operational conditions for using CTIPe as a mission planning tool for EVAs, since ACE averaged data would not be available in time to be used at or near real-time.

NASA CCMC provided the CTIPe data in .tar files for each day, each of which contained three output files for the day (in NetCDF file format), along with input files. Time steps, height grid values, latitude grid values, and longitude grid values from the output were also used. Since CTIPe produces one of each type of output file for each day, some of the model output is in a four-dimensional grid (i.e., a three-dimensional output grid for each fifteen minute output time step) within the data file. All output files were downloaded from the CCMC servers. NmF_2 and hmF_2 values were determined by finding the peak electron density values in the electron density

grids at each timestep and the height at which those peak values were found; this resulted in 2-D NmF_2 and hmF_2 grids with the same resolution as the electron density grids.

3.3.3 IFM.

All of the IFM runs for this effort were performed remotely on a USU computer with IFM and GAIM installed. To complete an IFM run, desired model output dates were modified in a text file, which was then read by the model. All model drivers were automatically downloaded and input into IFM.

Since the IFM model output acts as the baseline for the GAIM model upon which perturbations are applied using assimilated data, additional "warm-up" days were run outside the time period for each run as part of the process of running the GAIM models. IFM outputs files in the NetCDF format, similar to CTIPe; however, IFM produces a different output file at each fifteen minute time step. IFM-predicted NmF_2 and hmF_2 values were calculated in the same manner described in 3.3.2.

3.3.4 GAIM.

Like IFM, all GAIM runs were performed remotely on a USU computer with GAIM installed. Prior to executing a GAIM model run, a number of steps had to be completed to download and prepare data for assimilation into the model. The GAIM model had to be run for one day prior to the desired output time period, and IFM output had to exist for a day prior to that. So, if five days of model output were desired, GAIM had to be run for a total of six days, and IFM had to be run for a total of seven days.

In order to better understand the impact different data sources have on GAIM performance, GAIM was run in two different modes: with two data sources (GPS TEC

and ionosonde data), and with three data sources (GPS TEC, ionosonde data, and DMSP in-situ electron densities). The runs using two data sources are identified in this effort as GAIM 2, while the runs using three data sources are identified as GAIM 3. Additionally, GAIM 3 was run in forecast mode to create three, six, twelve, and twenty-four hour forecasts. GAIM 3 was chosen because it was assumed to perform the best due to the additional data assimilation source, particularly an in-situ electron density source. These forecast runs were included to potentially provide more options to NASA regarding EVA mission planning by examining how well GAIM can predict values in the future.

The first step in running GAIM is to prepare the input data for assimilation. This is done by executing a number of command line scripts created by USU that download GPS TEC, ionosonde, or DMSP data after modifying text files to reflect the days for which data is required. GPS TEC data is downloaded from NOAA, NASA, and UCSD data sources, and DMSP electron density data and ionosonde data are downloaded from NOAA. Next, the downloaded input data is reduced, or processed, into a format that GAIM can use through command line scripts. Further information about this process can be found in (*Scherliess et al.*, 2006). Additionally, these scripts determine the optimal number of those sources geographically to provide the best global coverage and write those sources to a text file. Those text files are then read by the GAIM program to determine which data to assimilate.

Configuration files must also be edited to specify which data sources will be assimilated, the time steps of the output, and whether the model will be run in forecast mode (and if so, what the forecast output time step will be). Then, the main GAIM scripts can be run. Like IFM, all GAIM output files are in NetCDF format with the date and time the output file is specified for in the filename. For this effort, forecast output files were identified by a suffix added to the filename. GAIM-predicted

NmF_2 and hmF_2 values were calculated in the same manner described in 3.3.2.

3.4 Importing and Interpolating Data

All data was imported into Matrix Lab software (MATLAB version 7.13.0.564) for analysis. Scripts were written for this effort to import, process, and interpolate (when necessary) FPMU and model output. These scripts are described below.

3.4.1 Binomial Filter.

First, FPMU and IRI datasets were imported into MatLAB. Then, all of the missing electron density and electron temperature data were removed, with the remaining "good" data for each parameter saved with its corresponding time and location values (i.e., sets of separate times/locations for electron density and electron temperature).

A binomial filter was then used to filter out noise in the FPMU data. This was done using a five-point filter with weights determined as outlined in (*Aubury and Luk*, 1995) and shown in Equation 1, where $FPMU_i$ represents a FPMU data point and $FPMU*_i$ represents the filtered values. The binomial filter approximates a Gaussian and provides a better low-pass filter than a simple moving average. Then, a filter was applied to remove data points where all five data points used in the binomial filter were not separated by one second each; this was done to ensure the filter was not applied across temporal "gaps" in FPMU data. This led to a slight reduction in the number of valid data points used. A five-weight filter was chosen to be large enough to smooth out fine noise and reduce the amount of points discarded from the analysis set. The resulting subset of valid FPMU time and location data was saved as in the previous manner and used for the rest of the processes described below.

$$FPMU*_i = \frac{FPMU_{i-2} + 4(FPMU_{i-1}) + 6(FPMU_i) + 4(FPMU_{i+1}) + FPMU_{i+2}}{16} \tag{5}$$

3.4.2 Interpolation and Data Processing.

Since CTIPe, IFM, and GAIM all produce three dimensional output, model-predicted electron densities and temperatures needed to be interpolated to the FPMU times and locations. Additionally, CTIPe, IFM and GAIM all produced output in 15 minute intervals for this effort for a total of 96 three-dimensional grids for a given day, while the FPMU outputs data at a cadence of roughly 1 Hz, when available. All interpolation and data processing was done in MatLAB.

CTIPe has a latitude limitation in its electron temperature output, with values of 0 K at $\pm$ 50° geomagnetic latitude. These values were excluded from all calculations.

Temporally, the filtered FPMU data was broken up into 15-minute periods of time (matching the output of the 3-D models) and compared to the previous model output (in time). For instance, FPMU data from both 1205 and 1210 UT would be compared to the 3-D model outputs from 1200 UT. This represents a more realistic scenario for the real-time use of the models operationally by NASA, with the most current real-time output used. Further, in most cases the ionosphere does not change significantly at a given point within a 15-minute period, with the exception of local dawn and dusk, while the ISS may encounter significant ionospheric environmental changes in that same period due to its high orbital speed.

Once the FPMU data was separated into 15-minute segments, FPMU latitudes, longitudes and heights within each 15-minute period were input into a 3-D linear interpolation scheme in Matlab, using Matlab's built-in "interp3" function. This produced an interpolated electron density, electron temperature, or Total Electron Con-

tent value at each FPMU location using the 3-D (or 2-D, in the case of TEC, hmF_2, and NmF_2) output from the closest previous 15-minute time step as described above. Height values were not required for the interpolation of TEC, hmF_2, or NmF_2 values because they do not vary with height. This interpolation scheme created interpolated model output for each FPMU electron temperature and density value, as well as TEC, NmF_2, and hmF_2 values for all of the times and locations where FPMU data existed.

3.5 Analyzing Model Performance

After all of the FPMU and model data was imported and interpolated, it was output to text files for further analysis by other Matlab utilities created for this effort. Additionally, the open source plotting program gnuplot (version 4.6) was used to create all of the plots in this effort.

3.5.1 Electron Densities, hmF_2,NmF_2, and Total Electron Content.

Electron densities were compared using mean absolute percent difference (MAPD), mean percent difference (MPD), and Pearson's correlation coefficient values as described below. Since TEC, hmF_2, and NmF_2 were not measured by the FPMU, analysis involving those parameters was limited to calculating and comparing average values. This helped identify overall trends and whether differences in electron densities between models were related to the models predicting an overall difference in the number of electrons or simply a different height distribution of the electrons.

3.5.2 Electron Temperatures.

Electron temperatures were compared in two different ways for this effort. First, all electron temperature models were compared to FPMU data using the methods previously described where model data exists. This resulted in some gaps in CTIPe

electron temperature values at high latitudes. Next, all the models were compared for latitudes ± 38° latitude, which is the largest latitude range that CTIPe has electron temperature data for. While this likely doesn't represent an operational scenario, it provides a way to directly compare model performance across the same times and locations.

3.6 Statistical Analysis

There are a myriad of different statistical methods that can be used to analyze the performance of a model relative to measured data. For this effort, mean absolute percent difference (MAPD), mean percent difference (MPD), and Pearsons product-moment correlation coefficient (r) were calculated between FPMU data and the models for each day. MAPE was used to determine the average percent error for a given day and shows which model produces output that most closely matches FPMU data, while the MPE values identify overall biases (i.e., positive or negative) present in the models. While root-mean-square errors values are commonly reported in similar validation efforts, they are omitted here because they do not provide meaningful information about the scale of the errors in relation to the FPMU data, which is the focus for ISS mission planning.

Lastly, Pearsons product-moment correlation coefficient provides a measure of how well each of the models correlates (linearly) to the FPMU data. This is similar to the method used by NASA for EVA mission planning as described in Chapter 2.

Further, each of these metrics was broken up by latitude region and local time of day to more closely examine model performance. Performance was evaluated by day for each run, and for each run as a whole. Additionally, to evaluate performance in a more general sense, statistics were calculated for the entire set of data.

3.6.1 MAPD and MPD.

In order to gain a quantitative understanding of the differences in FPMU and model values, percent difference values were calculated. Mean absolute percent difference (MAPD) was used to determine the mean error across the data subset evaluated (Equation 6). Smaller MAPD values are better, and indicate that the model predicted values are not significantly different than the FPMU measured values.

Mean percent difference (MPD) was also calculated to evaluate overall biases (positive or negative) in the models (Equation 7). By definition, MPD values are less than or equal to MAPD values in magnitude. It is important to look at both MPD and MAPD values because a small MPD value (in magnitude) does not necessarily correspond to a small MAPD value. A small MPD value (in magnitude) simply means that the model in question does not have a tendency to show a large bias. In general, a small bias is preferred. However, a MPD (bias) that is close in magnitude to the MAPD (average error) may be more easily correctable in the models, since that would indicate a nearly constant positive or negative bias and may be able to be somewhat fixed by multiplying model values by a correction factor.

$$MAPD = \frac{100}{n} \sum_{i=1}^{n} \left| \frac{FPMU_i - Model_i}{FPMU_i} \right| \tag{6}$$

$$MPD = \frac{100}{n} \sum_{i=1}^{n} \frac{FPMU_i - Model_i}{FPMU_i} \tag{7}$$

3.6.2 Correlation Coefficient.

In addition to MAPD and MPD, Pearson's Correlation Coefficient is useful because it evaluates how well model data correlates linearly to FPMU data. This is important because a consistent bias in one of the models could perhaps be overcome by a scaling factor if the model correlated strongly enough. Strong correlation

indicates the models are capturing the overall trends in the ionosphere.

This coefficient is given by the equation (*Navidi*, 2006):

$$r = \frac{\sum_{i=1}^{n} \left(FPMU_i - \overline{FPMU}\right)\left(Model_i - \overline{Model}\right)}{\sqrt{\sum_{i=1}^{n} \left(FPMU_i - \overline{FPMU}\right)^2} \sqrt{\sum_{i=1}^{n} \left(Model_i - \overline{Model}\right)^2}} \tag{8}$$

Correlation coefficient values can vary from -1 to 1. The higher the magnitude, the stronger the linear correlation. Zero values indicate the two data sets are completely uncorrelated. Sometimes the correlation coefficient value of a large set of data can be stronger than the correlation values of subsets of the same set of data; this can happen when outlier data points in the data set are poorly correlated and skew the subset of data. When included in a larger set of data, their overall affect on the correlation is diminished, which is why larger data sets tend to be better for evaluating correlation.

IV. Results

4.1 Chapter Overview

The results of the analysis methodology described in Chapter 3 are presented here. First, the performance of each of the models is described based on each run. Then, overall trends in the data are presented. Due to the large amount of information analyzed in this effort, only representative plots are provided here. Electron density and electron temperature plots and data not presented here are available upon request. Values highlighted in green represent the best performance values for a given period, while red values indicate the worst performance values. For correlation coefficient values, the strongest values are highlighted in green, while the weakest or most inversely correlated values are highlighted in red. For MAPD, the smallest values are highlighted in green, while the largest values are highlighted in red. Finally, the smallest absolute MPD values (i.e., the models with the smallest biases) are highlighted in green, while the largest magnitude MPD values are highlighted in red.

Electron temperature results are shown based on the overall data available to each model unless otherwise noted; due to limitations in CTIPe electron temperature coverage, the analysis for CTIPe used a smaller subset of data points than the other three models. However, for completeness all of the electron temperature models were evaluated using the least restrictive set of latitudes. The results of the analysis using a common subset of latitudes referred to as "CTIPe-restricted data" in this effort and available upon request. Differences between the two sets of metrics are mentioned if they are significant.

4.2 Overall Trends

In this section, trends in the overall electron temperature and electron density data sets are examined. This is done to provide an overall representation of model performance across many different geomagnetic and solar conditions. Then, in the sections that follow, model performance during specific geomagnetic and solar activity conditions will be examined and compared to the model performance as a whole. Average hmF_2, NmF_2, and TEC values across all days are presented in Table 2. All of the hmF_2 values are within 12 km of each other and are close to our nominal expected value of 300 km. IRI-12 predicted the lowest hmF_2, while IFM predicted the highest hmF_2. Additionally, the use of the DMSP data source in GAIM 3 did not significantly shift the F_2 peak compared to the GAIM 2 hmF_2 values, increasing it's height by 0.61 km on average. CTIPe predicted the lowest average NmF_2 and TEC values of all of the models, almost half that of IFM, which predicted the largest values. As a result, we would expect CTIPe to predict the lowest electron densities and IFM to predict the highest electron densities of all of the models.

Table 2. Overall average model-predicted hmF2, NmF2, and TEC values.

Model	**hmF2** (km)	**NmF2** (x $10^{11} m^{-3}$)	**TEC** (x $10^{16} m^{-2}$)
IRI-90	290.27	5.06	15.52
IRI-12	285.61	4.50	13.15
CTIPe	295.51	2.90	8.09
IFM	296.43	6.24	15.76
GAIM 2	293.35	5.70	15.31
GAIM 3	293.96	5.64	15.34
GAIM 3 3-hr	295.59	5.74	15.40
GAIM 3 6-hr	296.81	5.88	15.55
GAIM 3 12-hr	297.51	5.94	15.62
GAIM 3 24-hr	297.51	5.94	15.63

4.2.1 Electron Density.

Overall, GAIM 2 performed the best across all of the available electron density data with the strongest correlation (0.870) and the third lowest MAPD (57%), although GAIM 3 performed essentially just as well (Table 3). This result was expected because of GAIM's assimilative nature. All of the GAIM 3 forecasts showed strong correlation to FPMU values (greater than 0.828), although they tended to have the second largest MAPD values behind IFM, likely due to the fact they were forecasts. All the GAIM 3 forecasts had a positive bias in relation to the real-time GAIM models. The two physics-based models (IFM and CTIPe) performed the worst overall, although they still showed generally strong correlation as a whole (0.740 and 0.701, respectively). IFM had the largest MAPD by far at 95%, likely driven by its strong positive bias of 64%, which was somewhat expected from the $NmF_2$and TEC results.

All of the models except CTIPe tended to overestimate electron densities, which underestimated electron densities by 28% on average, partially due to the fact that it does not seem to model the Appleton Anomaly. IRI-12 showed very little positive bias overall (7%), while all of the other models tended to overestimate by at least 30%. While the GAIM 3 12 hour forecast tended to perform slightly worse than the GAIM 3 24 hour forecast, the differences were negligible.

Looking at diurnal trends, GAIM 2 and GAIM 3 performed the best by far during the daytime (Table 4). All of the GAIM models (including the forecasts) showed stronger correlation during the daytime than the other models, with strong correlation values of at least 0.841. CTIPe performed the worst during the daytime, with the lowest correlation (0.709) and the third highest MAPD (52%). CTIPe also showed a strong negative bias (MPD) during the daytime (-48%); CTIPe's poor performance during the daytime and its tendency to under predict electron densities were partially due to the fact that CTIPe does not seem to model the Appleton Anomaly, which

Table 3. Total performance of ionospheric model predicted electron density values in relation to FPMU data.

Model	Correlation (r)	MAPD (%)	MPD (%)
IRI-90	0.840	64	38
IRI-12	0.843	46	7
CTIPe	0.701	62	-28
IFM	0.740	95	64
GAIM 2	0.870	57	32
GAIM 3	0.867	56	30
GAIM 3 3-hr	0.839	66	41
GAIM 3 6-hr	0.830	71	48
GAIM 3 12-hr	0.828	75	52
GAIM 3 24-hr	0.830	74	52

produces a "double peak" in electron density, as shown in Figure 7. GAIM 2 and 3 had a very weak negative bias (less than 1%), while the rest of the models exhibited a positive bias during the daytime. Figures 8 and 9 show examples of good and bad model performance across many ISS orbits, respectively.

Table 4. Diurnal performance of ionospheric model predicted electron density values in relation to FPMU data.

	Day			Night		
	(r)	(%)	(%)	(r)	(%)	(%)
IRI-90	0.836	62	35	0.761	67	40
IRI-12	0.841	42	7	0.771	49	7
CTIPe	0.709	52	-48	0.484	72	-10
IFM	0.767	69	35	0.596	119	91
GAIM 2	0.881	33	-1	0.775	80	63
GAIM 3	0.878	33	0	0.773	77	59
GAIM 3 3-hr	0.851	44	13	0.722	86	67
GAIM 3 6-hr	0.843	50	20	0.714	92	74
GAIM 3 12-hr	0.841	52	23	0.713	96	79
GAIM 3 24-hr	0.843	51	22	0.716	96	80

At nighttime, GAIM 2 and GAIM 3 still had the best correlation, but its MAPD rose to at least 77% and it tended to over predict electron density values by at least 59%. IRI-12 performed the best at night, with the third strongest correlation (0.771) and the smallest MAPD (42%). IFM performed the worst at night, with

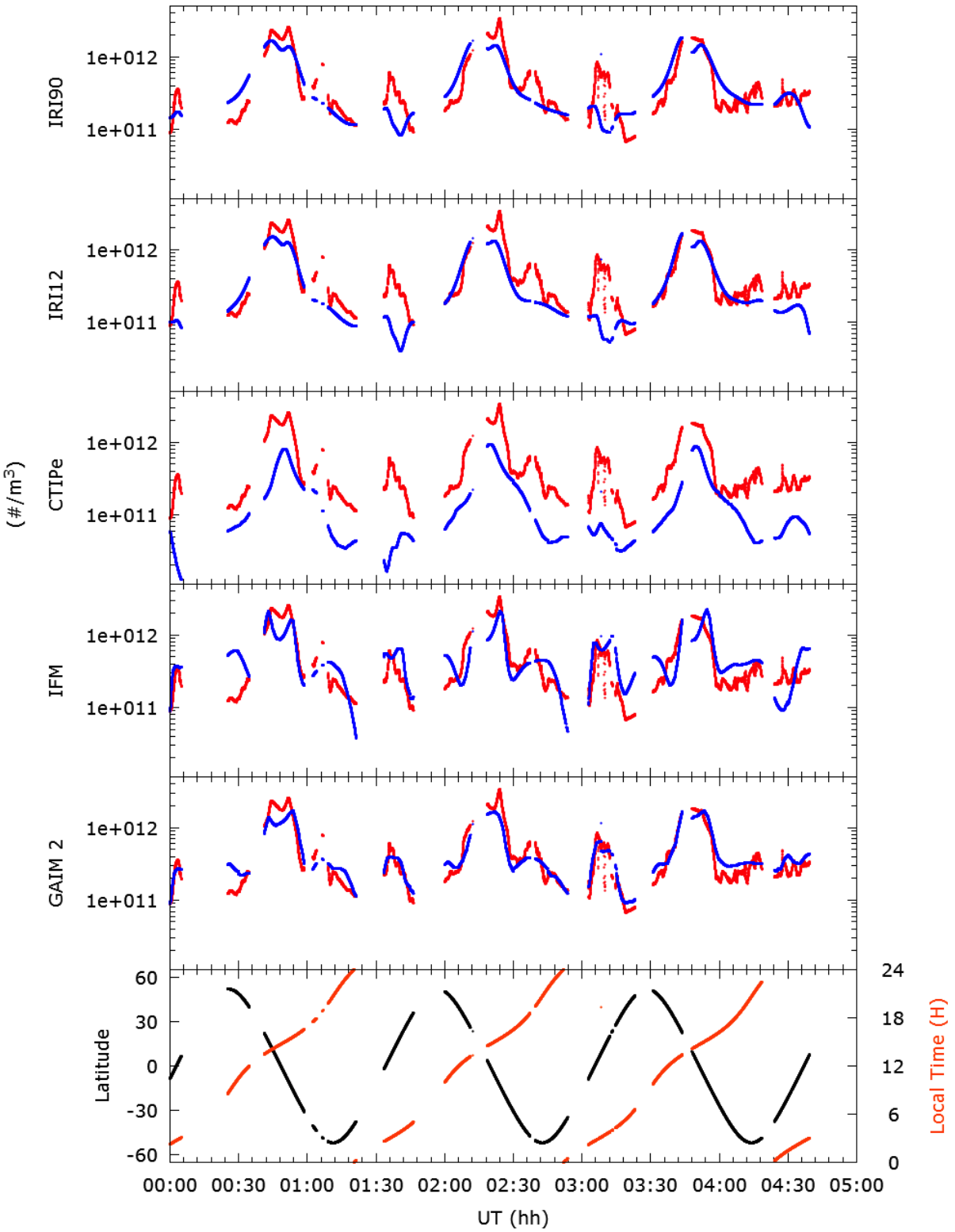

Figure 7. Model Predicted Electron Density Values versus FPMU Values for 7 April 2010 (during geomagnetic storming and low solar activity). Model values are in blue, FPMU values are in red. In bottom graph, local time is plotted in orange and latitude is plotted in black.

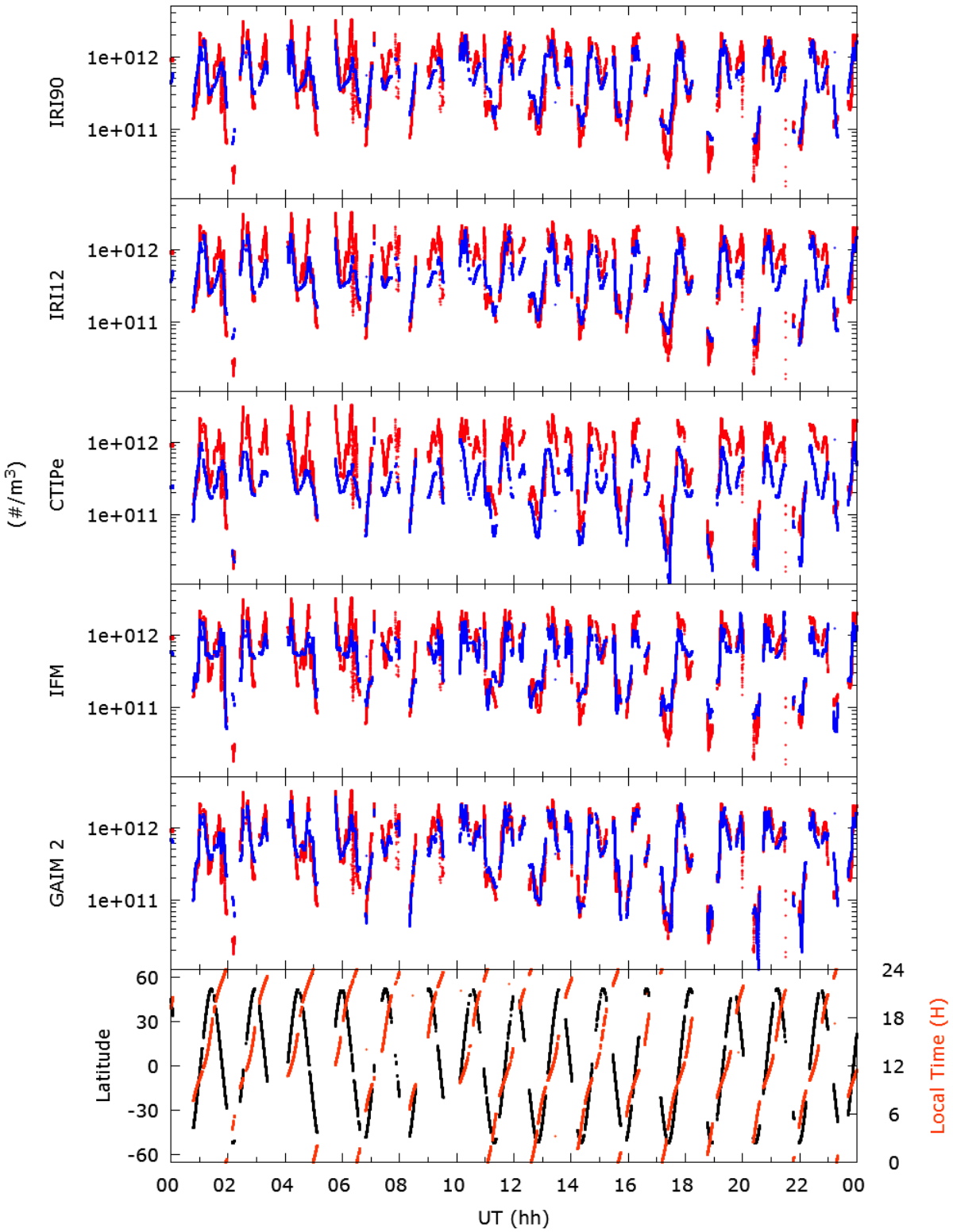

Figure 8. Model Predicted Electron Density Values versus FPMU Values for 5 May 2011 (during moderate geomagnetic and solar activity) showing good model performance overall. Model values are in blue, FPMU values are in red. In bottom graph, local time is plotted in orange and latitude is plotted in black.

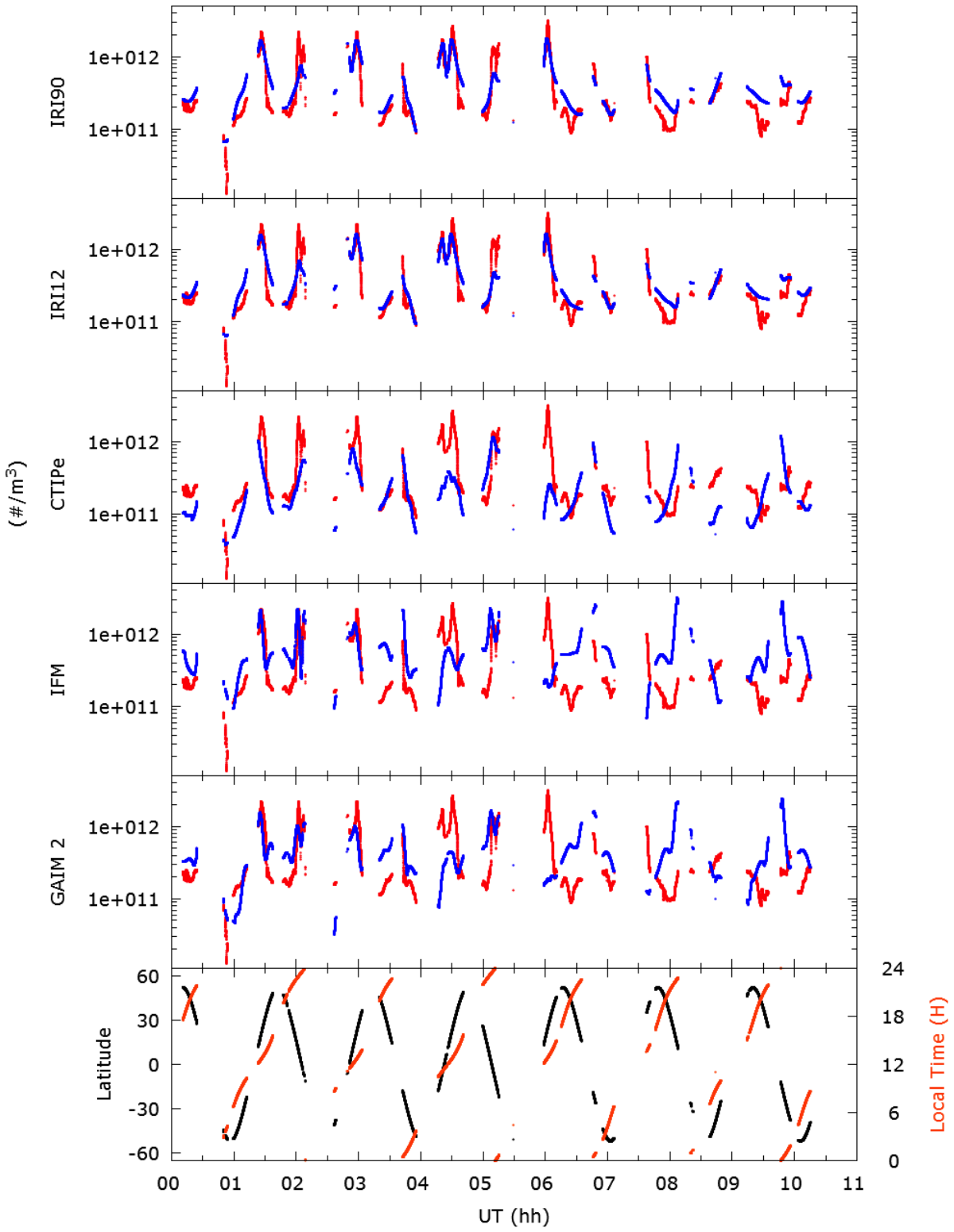

Figure 9. Model Predicted Electron Density Values versus FPMU Values for Day 64 2011 (during moderate geomagnetic and high solar activity) showing poor model performance overall. Model values are in blue, FPMU values are in red. In bottom graph, local time is plotted in orange and latitude is plotted in black.

the second weakest correlation (0.596) and the largest MAPD by far (119%). As expected, GAIM's overall performance trends followed IFM's, due to the fact IFM is used as a background for IFM. All of the models except CTIPe tended to overestimate electron density at night, particularly IFM (91%). While still exhibiting a negative bias, CTIPe's bias was much smaller in magnitude (10%) at night, when the Appleton Anomaly does not occur. Additionally, there was a significant increase in overall bias (greater than +38%) in all of the models except the two IRI models, likely due to their empirical, climatological nature. The weakened correlation and increase in positive bias at night is in part due to plasma bubbles and dawn density depletions created at night by equatorial spread F conditions. Currently, none of the models considered in this effort account for these effects due to the tenuous and volatile nature of plasma bubbles as well as the spatial resolution of the three dimensional models.

Regionally, IRI-12 performed the best at low-latitudes, although GAIM 2 and GAIM 3 had slightly stronger correlation values (but much larger MAPD values as well), as shown in Table 5. Again all of the models except CTIPe showed a positive bias, with IFM and GAIM exhibiting the strongest positive bias. CTIPe and IFM performed the worst overall at low latitudes, with the two weakest correlation values and the two highest MAPD values.

At mid-latitudes, GAIM 3 performed the best, showing the strongest correlation (0.870) and the second smallest MAPD (46%). CTIPe and the GAIM models showed an improvement in performance at mid-latitudes, while IFM and the IRI models exhibited a weaker correlation (but smaller MAPD) at mid-latitudes. This decrease in MAPD was likely due to the lack of plasma bubbles and the Appleton Anomaly in the mid-latitude region, which the models often struggled to accurately predict. IFM performed the worst overall at mid-latitudes, with the weakest correlation (0.643) and the largest MAPD (90%). All of the models except CTIPe again showed a positive

Table 5. Regional performance of ionospheric model predicted electron density values in relation to FPMU data.

Model	Low Latitude ($\|\Lambda\| \leq 30°$)			Mid Latitude ($\|\Lambda\| > 30°$)		
	Corr. (r)	**MAPD** (%)	**MPD** (%)	**Corr.** (r)	**MAPD** (%)	**MPD** (%)
IRI-90	0.805	71	36	0.768	59	39
IRI-12	0.807	54	5	0.787	39	8
CTIPe	0.617	78	-7	0.727	51	-44
IFM	0.690	102	55	0.643	90	70
GAIM 2	0.831	72	45	0.870	47	22
GAIM 3	0.827	70	42	0.870	46	21
GAIM 3 3-hr	0.795	78	47	0.809	57	36
GAIM 3 6-hr	0.787	82	50	0.791	64	46
GAIM 3 12-hr	0.784	84	52	0.787	68	52
GAIM 3 24-hr	0.785	84	53	0.793	67	51

bias at mid-latitudes, with a slight increase in positive bias for IFM and the IRI models at mid-latitudes (compared to low-latitudes).

4.2.2 Electron Temperature.

IRI-12 performed the best of all of the models at predicting electron temperatures, with a moderate correlation of 0.697 and MAPD of 22%; IRI-90 performed essentially the same with a slightly lower correlation and slightly higher MAPD (Table 6). IFM performed the worst of all of the models, which was somewhat expected given the age of its electron temperature model (*Schunk*, 2012). It had a low correlation of 0.328 (but a slightly stronger 0.510 using the CTIPe-restricted data set) and a MAPD of 42%. Other than the aforementioned difference in IFM correlation, there was a negligible difference between using the full set of data and the CTIPe-restricted set of ephemeris data. CTIPe was the only model to exhibit a positive bias, albeit a very weak one (1%). These model bias values display the previously mentioned inverse relationship between electron density and electron temperature; the model that predicted the lowest electron temperature values (IFM) is also the model that

predicted the highest electron density values on average. Conversely, the model that tended to under predict electron densities the most (CTIPe) was the only one with a positive bias. Figures 10 and 11 show examples of good and bad model performance across many ISS orbits, respectively.

Table 6. Total performance of ionospheric model predicted electron temperature values in relation to FPMU data.

Model	Correlation (r)	MAPD (%)	MPD (%)
IRI-90	0.700	24	-19
IRI-12	0.697	22	-19
CTIPe	0.567	24	1
IFM	0.328	42	-40

All of the models performed worse during the daytime, due to the fact that electron temperatures fluctuate the most during the daytime, when electron densities also fluctuate the most. The best model correlation coefficient value (IRI-90) was a weak 0.357 (Table 7). IRI-90 performed the best overall during the day, also producing the lowest MAPD (17%). IFM again performed the worst, with very weak correlation (0.064) and the highest MAPD (42%). IFM's poor daytime performance was likely related to its tendency to over predict electron density values then, leading to larger electron cooling rates. CTIPe exhibited a negligible negative bias, while the other models tended to under predict electron temperatures by at least 10%.

Table 7. Diurnal performance of ionospheric model predicted electron temperature values in relation to FPMU data.

	Day			Night		
Model	**Corr.** (r)	**MAPD** (%)	**MPD** (%)	**Corr.** (r)	**MAPD** (%)	**MPD** (%)
IRI-90	0.357	17	-10	0.499	31	-28
IRI-12	0.335	19	-16	0.532	26	-22
CTIPe	0.179	21	-1	0.327	26	3
IFM	0.064	48	-47	0.233	36	-32

All of the models showed better correlation at night, when IRI-12 performed the

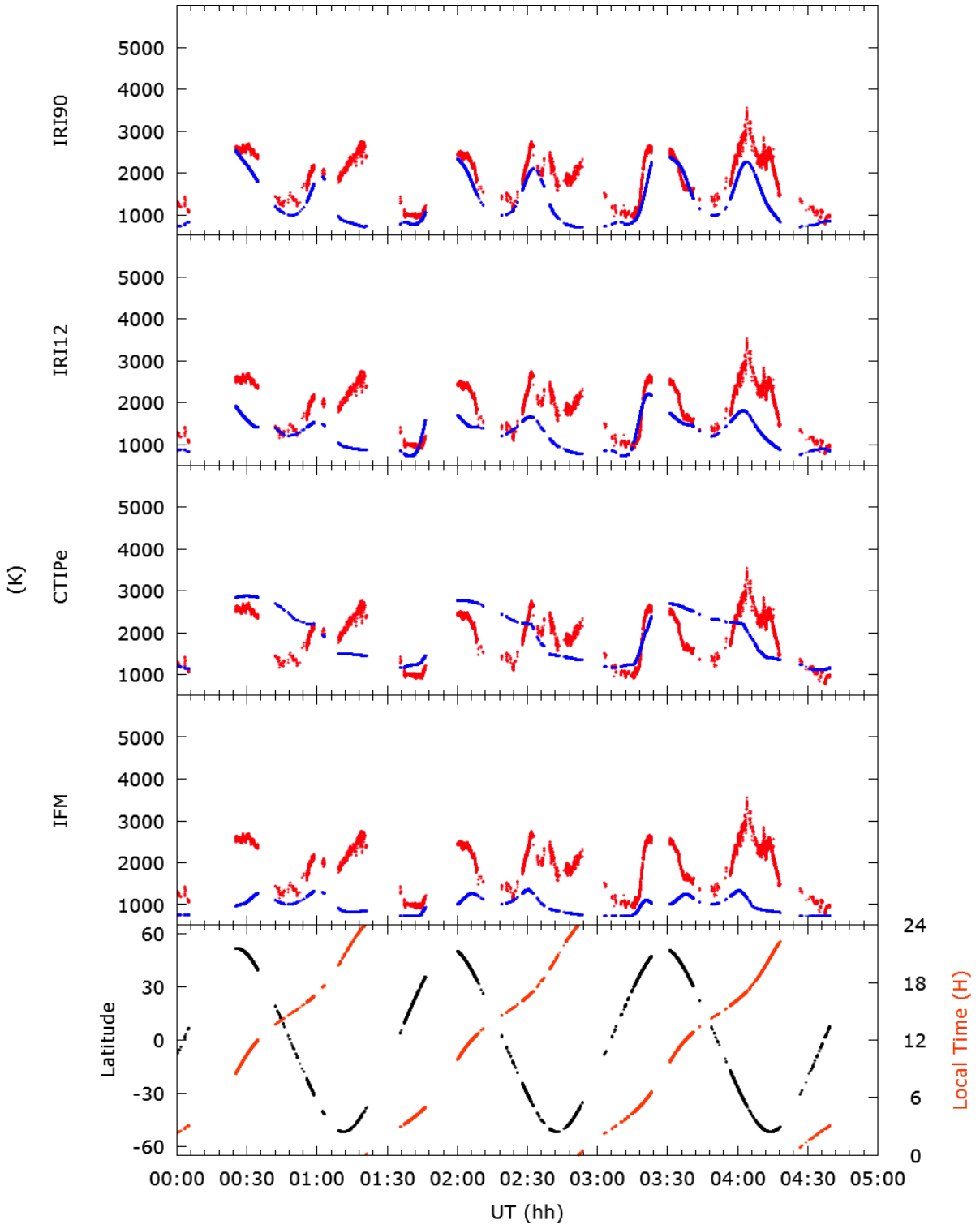

Figure 10. Model Predicted Electron Temperature Values versus FPMU Values for 7 April 2010 (during geomagnetic storming and low solar activity) showing good model performance overall. Model values are in blue, FPMU values are in red. In bottom graph, local time is plotted in orange and latitude is plotted in black.

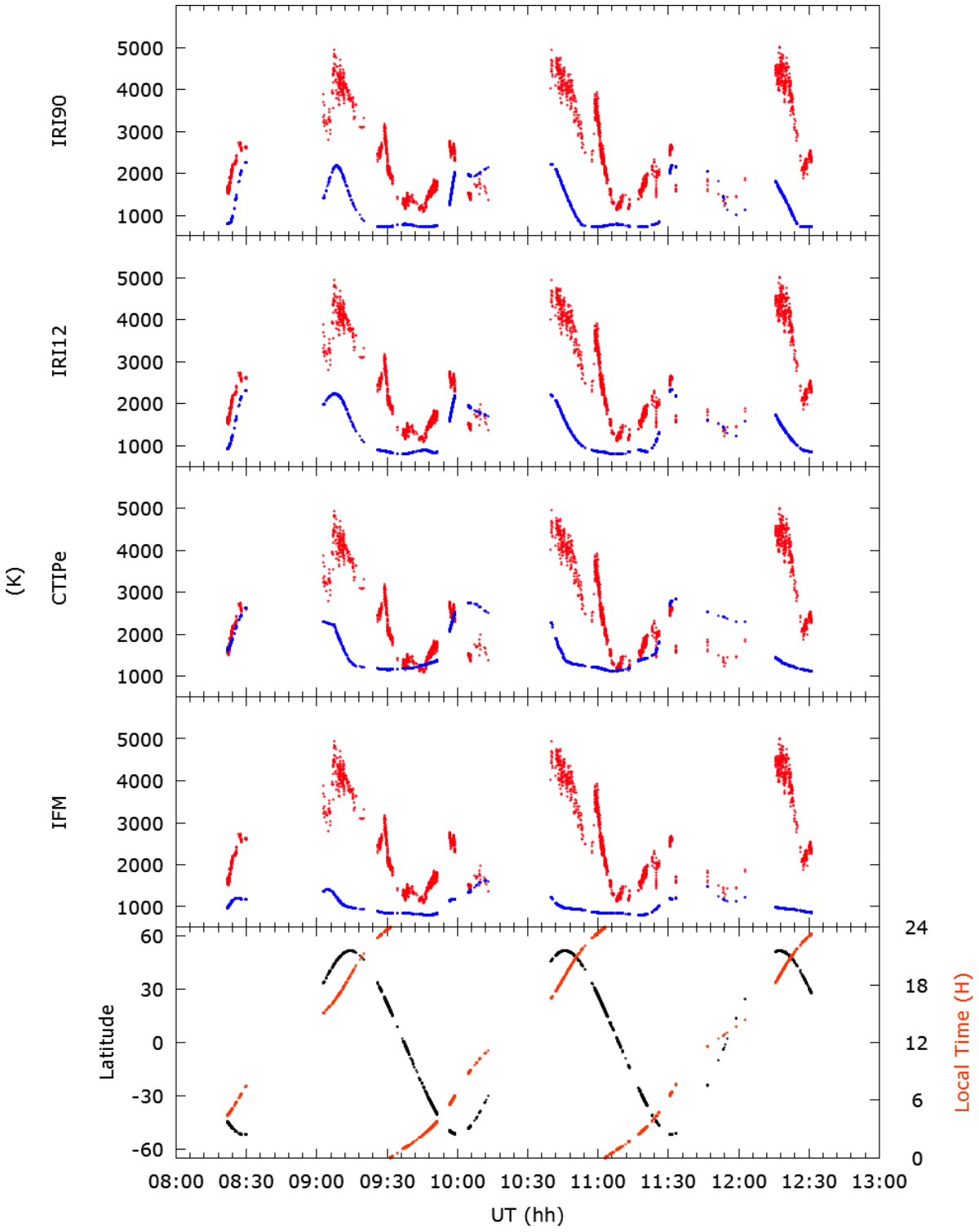

Figure 11. Model Predicted Electron Temperature Values versus FPMU Values for 1 March 2011 (during moderate geomagnetic and high solar activity) showing poor model performance overall. Model values are in blue, FPMU values are in red. In bottom graph, local time is plotted in orange and latitude is plotted in black.

best with the strongest correlation (0.532) and and lowest MAPD (27%). IFM again performed the worst overall at night. The IRI models had a larger negative bias at night, while the magnitude of IFM's negative bias decreased at night. This decrease in negative bias at night (when IFM tended to over predict electron density values more than during the daytime) was likely due to the direct relationship between temperature and scale height. At night, electron densities are greatly diminished, so the large cooling rates from collisions with relatively cold ions that dominate during the day are no longer as important. As a result, scale height plays a larger role in determining electron densities (since electron production essentially goes away at night), and as scale height increases, densities decrease more slowly with altitude, leading to larger densities just above the F2 peak. However, the night time plasma bubbles seen in the electron density data had a large effect on the electron density MAPD and MPD values during the night time and could have skewed the apparent effect of scale height, since plasma bubble effects were not seen in the electron temperature data.

Regionally, IRI-12 performed the best of the models at low latitudes, attaining the strongest correlation (0.710) and the second lowest MAPD value (27%), as seen in Table 8. CTIPe had the smallest MAPD (25%), but had the weakest correlation of the models at low latitudes (0.502). IFM again had the largest MAPD (34%). Similarly, all of the models showed a negative bias, while CTIPe had a slight positive bias (6%). All of the models except CTIPe showed stronger correlation at low latitudes, even though all of the models except IFM had larger MAPD values there than at mid-latitudes.

At mid-latitudes, IFM performed the worst overall, showing weak correlation (0.215) and a MAPD nearly twice as large as the other models (45%). Correlation improved in IFM to 0.429 when using the CTIPe-restricted set of ISS ephemeris data,

Table 8. Regional performance of ionospheric model predicted electron temperature values in relation to FPMU data.

Model	Low Latitude ($\|\Lambda\| \leq 30°$)			Mid Latitude ($\|\Lambda\| > 30°$)		
	Corr. (r)	**MAPD** (%)	**MPD** (%)	**Corr.** (r)	**MAPD** (%)	**MPD** (%)
IRI-90	0.676	32	-30	0.623	21	-14
IRI-12	0.710	27	-26	0.606	20	-16
CTIPe	0.502	25	6	0.529	23	-1
IFM	0.592	34	-33	0.215	45	-42

as well as a negligible 2% decrease in MAPD. IFM's change in performance at mid-latitudes (worsening with increasing latitude) is likely due to its mid/high-latitude electron temperature model and the"blending" region that overlaps with much of the mid-latitude region considered here. Again the overall inverse relationship between electron density and electron temperature is seen in IFM, which tended to over predict electron densities more at mid-latitudes and under predict electron temperatures more there. IRI-90 performed the best at mid-latitudes with the strongest correlation (0.630) and a MAPD value of 20%, although IRI-12 performed essentially the same. The general latitude trends seen in the regional electron density performance held here, with CTIPe's performance improving at mid latitudes (with the caveat that it couldn't predict electron temperature values across all of the mid latitudes considered by the other models), and all of the other models exhibiting worse performance at mid-latitudes than at low latitudes. CTIPe showed the most constant performance across both regions, but the two IRI models still performed better in both.

4.3 Run 1 Results - Low Geomagnetic and Solar Activity

Run 1 represented solar and geomagnetic quiet conditions and occurred during 10-12 September 2007. The F10.7 index stayed relatively constant at 67 for the duration of the period, while the Kp index remained at or below 1 (Figure 12). All of the models seemed to struggle the most with this combination of geomagnetic and solar activity,

likely due to the deep solar minimum experienced during this period. The deep solar minimum of 2007-2008 was a very unique period. As a result of the extremely low solar EUV flux, the lowest thermospheric densities ever recorded occurred during this period (*Emmert et al.*, 2010). Additionally, there was generally poor correlation between EUV irradiance and the F10.7 index (*Chen et al.*, 2011), which all of the models use as a proxy for solar activity. Analysis by *Bilitza et al.* (2012) suggests that there was a fundamental change in ionospheric composition during this period, especially in the topside ionosphere profile, due to the decreased densities and EUV flux.

Additionally, this period of solar minimum was unique because a previously undiscovered plasma depletion phenomenon was observed. This phenomenon, described by *Huang et al.* (2009), is the presence of broad plasma depletions (much larger in horizontal extent than plasma bubbles) at night near the equator. Since they are so broad, they are not formed in the same way as plasma bubbles, but it is not yet fully understood what causes them. However, it is believed that they are a result of cooling in the ionosphere and thermosphere, especially in the equatorial region (*Huang et al.*, 2009). Based on analyzing electron density plots during this period, the FPMU encountered these depletions during most of its orbits during this run and during many of the orbits during Run 2.

Average hmF_2, NmF_2, and TEC values for the period are presented in Table 9, and show some distinct differences in relation to the overall averages. Here we see the predicted NmF_2 and TEC values are much lower than the overall averages, with NmF_2 and TEC values nearly reduced by half as a result of the low F10.7 and Kp index values. Here IFM predicted the largest NmF_2, while IRI-12 predicted the smallest. For TEC, CTIPe and IRI-90 predicted the smallest and largest TEC values, respectively, suggesting significant differences in the relative electron density

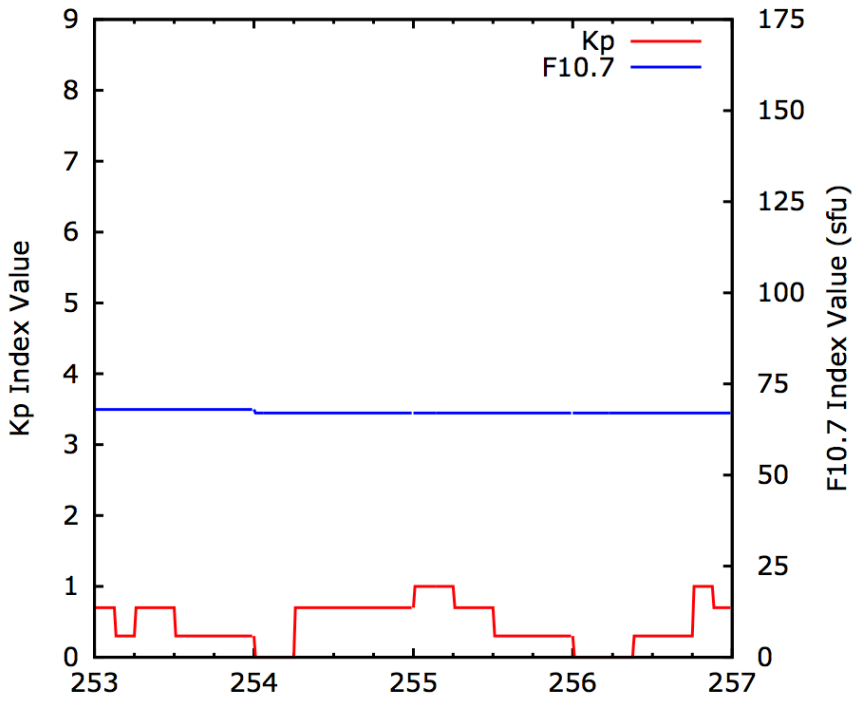

Figure 12. Run 1 Kp and F10.7 Index Values for 10-13 September 2007 ($sfu = 10^{-22} W\ m^{-2}\ s$)**.**

distributions between the models. Lastly, the predicted hmF_2 values are much lower (approximately 20 km lower than the overall average), due to the general decrease in electron densities predicted during this period.

4.3.1 Electron Density.

Electron density MAPD, MPD and correlation coefficients are presented in Table 10. All of the models overestimated electron densities during this period by greater than 64%. IFM had the worst performance, with a MAPD value of 170% for the period. IFM also had the second weakest correlation for the period (0.522), while CTIPe had the weakest correlation (0.391) and third highest MAPD values.

As a whole, IRI-12 and GAIM 3 performed the best during this period of solar and geomagnetic quiet conditions, with GAIM 3 posting the second strongest correlation overall (0.686) and the second lowest lowest MAPD (84.00%). The use of an additional

Table 9. Run 1 average model-predicted hmF2, NmF2, and TEC values.

Model	hmF2 (km)	NmF2 (x $10^{11} m^{-3}$)	TEC (x $10^{16} m^{-2}$)
IRI-90	274.54	3.18	10.01
IRI-12	270.90	2.71	7.82
CTIPe	250.81	2.87	6.20
IFM	272.32	4.37	8.80
GAIM 2	266.35	3.05	6.82
GAIM 3	267.64	2.90	6.92
GAIM 3 3-hr	268.99	3.13	7.31
GAIM 3 6-hr	270.66	3.43	7.73
GAIM 3 12-hr	272.17	3.55	7.82
GAIM 3 24-hr	272.24	3.55	7.84

GAIM data source in GAIM 3 brought a slight reduction in MAPD (6.3%) and a negligible difference in correlation when compared to GAIM 2. IRI-12 had the lowest MAPD value (64%) but had a weaker correlation value (0.620).

Unsurprisingly, all of the GAIM forecasts performed better in both MAPD and correlation than IFM (since IFM is used as the "background" for the assimilated data), and tended to perform worse as the forecast increased. This trend can be seen in general throughout all of the runs, with the exception that the 24-hour GAIM 3 forecast had a slightly smaller MAPD value (0.94% difference) than the 12-hour forecast.

Table 10. Run 1 performance of ionospheric model predicted electron density values in relation to FPMU data.

Model	Correlation (r)	MAPD (%)	MPD (%)
IRI-90	0.593	117	113
IRI-12	0.615	65	56
CTIPe	0.384	107	80
IFM	0.508	171	155
GAIM 2	0.684	87	78
GAIM 3	0.683	81	71
GAIM 3 3-hr	0.607	99	90
GAIM 3 6-hr	0.580	117	108
GAIM 3 12-hr	0.575	125	117
GAIM 3 24-hr	0.579	124	117

Looking at diurnal trends (Table 11), all of the models performed significantly worse during local nighttime conditions, with IFM and CTIPe posting MAPD values of 202% and 154%, respectively. All of the models exhibited a strong positive bias at night as well. The two physics-based models also had weak negative correlation coefficient values (-0.090 for CTIPe and -0.041 for IFM), indicating a weak inverse correlation and very bad correlation to FPMU electron density values at night during solar and geomagnetic quiet conditions. IRI-12 performed the best of the models during the nighttime, although it still showed weak correlation (0.421) and had a high MAPD value (65%). In fact, all of the models except IRI-12 had MAPD values greater than 110% during the nighttime and correlation coefficient values weaker than 0.325. A significant reason the models didn't perform well at night was due to broad plasma depletions, which the FPMU measured on most of the orbits during this run. An example of a broad plasma depletion is provided in Figure 13 at approximately 0400 UT. None of the models currently account for these depletions, as evidenced in the plot.

Table 11. Diurnal Run 1 performance of ionospheric model predicted electron density values in relation to FPMU data.

Model	Day			Night		
	Corr. (r)	**MAPD** (%)	**MPD** (%)	**Corr.** (r)	**MAPD** (%)	**MPD** (%)
IRI-90	0.574	111	108	0.264	121	115
IRI-12	0.592	64	60	0.421	65	53
CTIPe	0.459	31	-7	-0.090	154	135
IFM	0.496	122	116	-0.041	202	179
GAIM 2	0.696	33	19	0.325	121	116
GAIM 3	0.693	33	19	0.308	111	103
GAIM 3 3-hr	0.598	56	46	0.113	127	117
GAIM 3 6-hr	0.571	74	67	0.058	143	134
GAIM 3 12-hr	0.569	79	73	0.030	153	144
GAIM 3 24-hr	0.571	77	71	0.034	154	146

GAIM 2 and GAIM 3 performed the best during the daytime (Table 11), with the

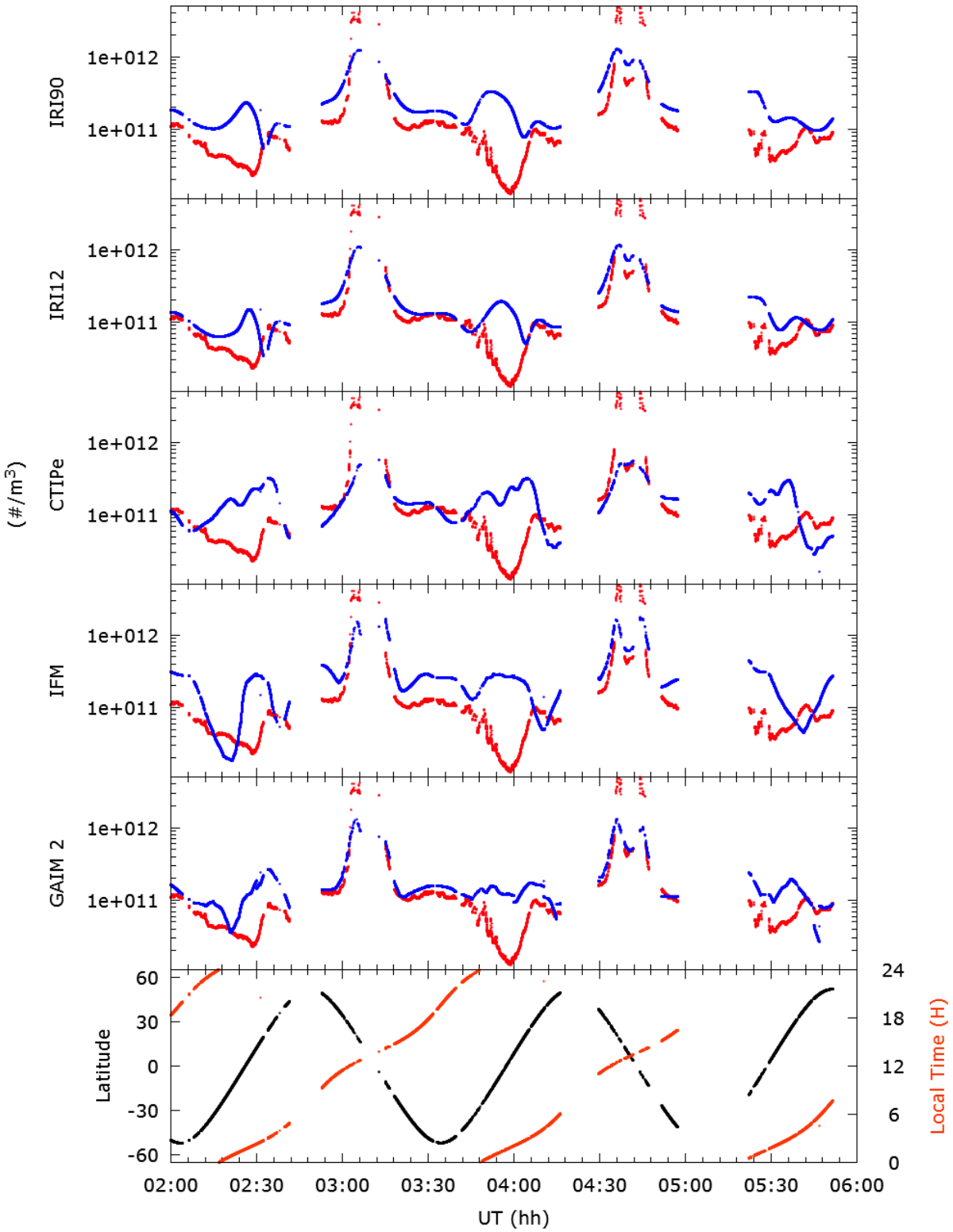

Figure 13. Model Predicted Electron Density Values versus FPMU Values for 12 September 2007 (during low geomagnetic and solar activity). Model values are in blue, FPMU values are in red. In bottom graph, local time is plotted in orange and latitude is plotted in black. Note the broad plasma depletion that occurs around 0400 UT that none of the models account for.

second and third lowest MAPD values (33%) and the strongest correlation (0.696 and 0.693, respectively). IFM performed the worst during the daytime, with an MAPD value of 122% and a correlation of 0.496. CTIPe had both the best MAPD value (31%) and the weakest correlation value (0.459), indicating that even though it had the lowest errors, the other models were tracking the trends better. To better illustrate the drastic diurnal difference in performance (and the effect of plasma depletions), CTIPe's weak correlation value during the day was still better than the strongest correlation during the nighttime (0.421, by IRI-12). The poor correlation shown by all of the models during the daytime is likely due to both discontinuous high FPMU electron density values near the Appleton Anomaly and the models inability to accurately predict solar production rates during such a low solar minimum.

The effects of plasma depletions on the model performance were clearly evident in the regional analysis as well. All of the models also had much higher MAPD values at low latitudes where plasma depletions occur (Table 12), with all models averaging at least a 95% absolute difference value. IFM and CTIPe had MAPD values greater than 228%. GAIM 3 performed the best overall at low latitudes, showing the strongest correlation (0.702) and the second lowest MAPD value (128%), while CTIPe performed the worst, with the weakest correlation (0.390) and the second highest MAPD value (228%).

GAIM 3 had the strongest correlation at low latitudes (0.702), but its correlation weakened significantly at mid latitudes (0.470), even though its MAPD values decreased by more than a factor of 2 there. IFM and all of the other GAIM models showed a similar trend. Conversely, IRI-90, IRI-12 and CTIPe all showed stronger correlation at mid-latitudes than at low-latitudes, with IRI-12 showing the strongest correlation (0.766) and second lowest MAPD value (46%) at mid-latitudes. IFM did the worst at mid-latitudes, with the weakest correlation (0.430) and the highest

Table 12. Regional Run 1 performance of ionospheric model predicted electron density values in relation to FPMU data.

Model	Low Latitude ($\|\Lambda\| \leq 30°$)			Mid Latitude ($\|\Lambda\| > 30°$)		
	Corr. (r)	**MAPD** (%)	**MPD** (%)	**Corr.** (r)	**MAPD** (%)	**MPD** (%)
IRI-90	0.592	172	167	0.731	84	80
IRI-12	0.610	96	85	0.766	46	38
CTIPe	0.390	228	216	0.518	33	-3
IFM	0.504	248	215	0.430	125	118
GAIM 2	0.702	138	130	0.471	56	47
GAIM 3	0.700	128	119	0.512	52	41
GAIM 3 3-hr	0.611	151	138	0.478	68	61
GAIM 3 6-hr	0.581	172	158	0.473	83	78
GAIM 3 12-hr	0.576	182	167	0.472	90	86
GAIM 3 24-hr	0.579	184	170	0.485	88	84

MAPD value (125%). CTIPe had a slight negative bias of -3% at mid latitudes, while the rest of the models exhibited a positive bias. This negative bias at mid-latitudes is likely due to the relative lack of plasma depletions at mid-latitudes, especially since CTIPe showed the largest positive bias (216%) at low latitudes. GAIM 3 (and all of the GAIM 3 forecasts) showed stronger correlation at mid-latitudes than GAIM 2, perhaps due to DMSP data coverage.

4.3.2 Electron Temperature.

In contrast to the electron density performance during this period, the models performed better during this period, showing stronger correlation than they did as a whole across all runs (Table 13). All models tended to underestimate FPMU electron temperature values across the period by at least 15%. CTIPe performed the best overall, showing the strongest correlation (0.859) by far and third lowest MAPD value (24%). IRI-90 had showed stronger correlation and had a smaller MAPD value than IRI-12. IFM had the highest MAPD value (47%) and the second weakest correlation coefficient (0.692). IRI-12 had the worst correlation of all of the models (0.685), even

though it had the second best MAPD values.

Table 13. Run 1 performance of ionospheric model predicted electron temperature values in relation to FPMU data.

Model	Correlation (r)	MAPD (%)	MPD (%)
IRI-90	0.743	20	-14
IRI-12	0.685	21	-17
CTIPe	0.859	24	-23
IFM	0.692	47	-47

Looking at daytime performance, all of the models exhibited very weak correlation, with all but IRI-90 having a correlation of less than 0.10 (Table 14). IFM performed the worst, with a very weak correlation of 0.020 and a MAPD value of 50%, while IRI-90 did the best with the strongest (but still weak) correlation of 0.307 and the lowest MAPD value (19%). All of the models had weaker day time correlation and stronger day time negative biases during this period, likely due to over predicting electron densities more than in the overall results during this run.

Table 14. Run 1 Diurnal performance of ionospheric model predicted electron temperature values in relation to FPMU data.

	Day			Night		
Model	**Corr.** (r)	**MAPD** (%)	**MPD** (%)	**Corr.** (r)	**MAPD** (%)	**MPD** (%)
IRI-90	0.307	19	-13	0.752	22	-17
IRI-12	0.071	22	-19	0.736	20	-12
CTIPe	0.099	25	-23	0.734	22	-22
IFM	0.020	50	-50	0.628	40	-40

At night, all of the models performed much better; each model had a correlation of at least 0.628. IRI-90 again did the best overall with the strongest correlation (0.752) and the second lowest MAPD value (22%), while IFM again did the worst, with a correlation of 0.628 and a MAPD of 40%. All of the models showed a negative bias for both day and night. While the models exhibited very poor correlation during the day time (in general and compared to the night time values), the MAPD and MPD

values improved by only a small amount during night time. This indicates that the models were not accurately capturing the trends in the FPMU electron temperature data in the daytime, even though the errors were relatively low. Additionally, the general improvement in performance at night during this period indicates that the larger electron density errors observed at night during this period were largely due to the higher incidence of dawn density depletions.

While there was a distinct difference between day and nighttime performance, the performance in each of the latitude regions was largely similar, although all of the models except CTIPe tended to perform better at low latitudes, consistent with the trend seen in the overall data (Table 15). At low latitudes, all of the models showed strong correlation values of at least 0.768 (IRI-90). CTIPe performed the best, with a correlation of 0.847 and a MAPD of 21%. IFM had the second strongest correlation (0.825), but again had the highest MAPD (43%). IRI-90 performed the worst at low latitudes, with the weakest correlation (0.768) and the second largest MAPD (32%).

Table 15. Run 1 Regional performance of ionospheric model predicted electron temperature values in relation to FPMU data.

Model	Low Latitude ($\|\Lambda\| \leq 30°$)			Mid Latitude ($\|\Lambda\| > 30°$)		
	Corr. (r)	**MAPD** (%)	**MPD** (%)	**Corr.** (r)	**MAPD** (%)	**MPD** (%)
IRI-90	0.768	32	-31	0.774	15	-7
IRI-12	0.772	25	-24	0.640	20	-14
CTIPe	0.847	21	-19	0.892	25	-25
IFM	0.825	43	-43	0.655	48	-48

At mid-latitudes, CTIPe showed very strong correlation (0.892), but had the third highest MAPD (25%). IFM's correlation slightly weakened at mid-latitudes to 0.665, and again had the highest MAPD (48%) and worst performance overall.

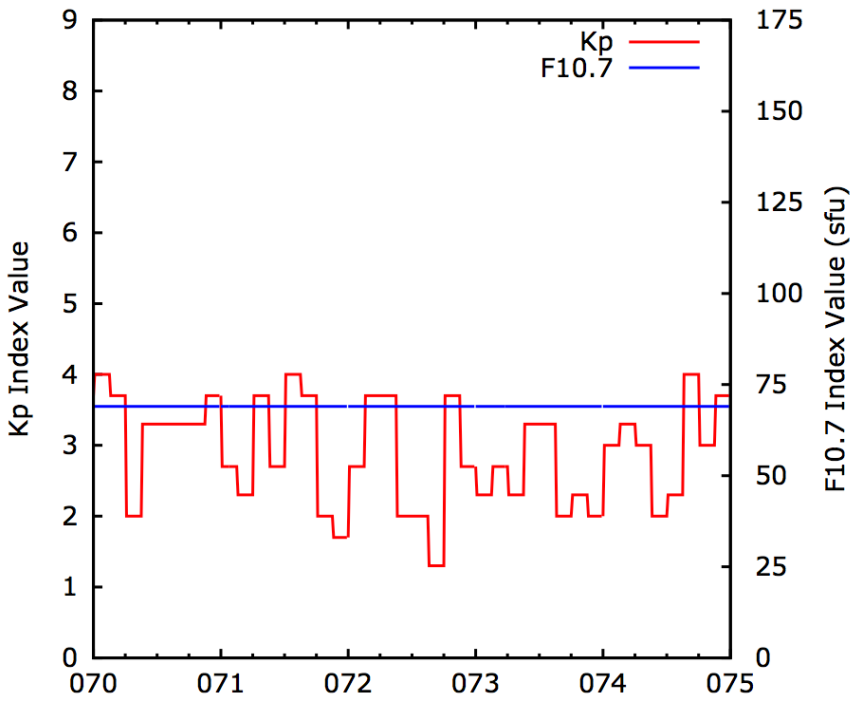

Figure 14. Run 2 Kp and F10.7 Index Values for 10-14 March 2008 ($sfu = 10^{-22} W\ m^{-2}\ s$).

4.4 Run 2 Results - Low Solar Activity and Moderate Geomagnetic Storming

Run 2 occurred during 10-14 March 2008 and represented low solar activity and moderate geomagnetic storming. F10.7 values for the period stayed constant at 68 for the entire period, while Kp index values fluctuated between 1+ and 4 (Figure 14).

Average hmF_2, NmF_2, and TEC values for the period are presented in Table 16. Here we see slightly larger NmF_2 and TEC values than in Run 1 due to the increased geomagnetic activity, but they are still well below the overall averages due to the deep solar minimum during this period. CTIPe again predicted the lowest NmF_2 and TEC values, and IFM and IRI-90 predicted the largest NmF_2 and TEC values, respectively. CTIPe also predicted the lowest hmF_2, while GAIM 3 24-hr predicted the highest value.

Table 16. Run 2 average model-predicted hmF2, NmF2, and TEC values.

Model	hmF2 (km)	NmF2 (x $10^{11} m^{-3}$)	TEC (x $10^{16} m^{-2}$)
IRI-90	282.15	4.13	13.36
IRI-12	275.84	3.18	9.78
CTIPe	275.53	1.99	4.94
IFM	281.70	4.24	9.62
GAIM 2	279.44	3.73	9.27
GAIM 3	280.35	3.56	9.33
GAIM 3 3-hr	282.11	3.68	9.33
GAIM 3 6-hr	283.04	3.84	9.47
GAIM 3 12-hr	283.62	3.94	9.54
GAIM 3 24-hr	283.69	3.96	9.73

4.4.1 Electron Density.

Electron density MAPD, MPD and correlation coefficients for Run 2 are presented in Table 17. GAIM 3 performed the best of all the models in these conditions, with the strongest correlation (0.707) and the second lowest MAPD (44%). All of the models showed worse correlation during Run 2 than across all data, again likely due to the fact that the models performed so poorly during the deep solar minimum of 2007-2008. CTIPe performed the worst of all of the models, with a correlation of 0.528 and a MAPD of 52%. All of the GAIM 3 forecasts performed better than CTIPe and IRI-90, with stronger correlation and slightly larger MAPD values than CTIPe (but still below IRI-90). As seen in the overall results, all of the models except CTIPe tended to over predict electron density values.

Looking at diurnal trends (Table 18), GAIM 3 performed the best during the daytime, as in the overall set of Run 2 data, with both the strongest correlation (0.724) and the lowest MAPD value. CTIPe performed the worst overall with a correlation of 0.565, while IRI-90 had the highest MAPD (88%). IFM actually showed stronger correlation than CTIPe and both IRI models during the daytime. All of the models performed worse at night than during the day, again due to plasma depletions

Table 17. Run 2 performance of ionospheric model predicted electron density values in relation to FPMU data.

Model	Correlation (r)	MAPD (%)	MPD (%)
IRI-90	0.647	72	62
IRI-12	0.661	40	11
CTIPe	0.528	52	-44
IFM	0.610	71	45
GAIM 2	0.699	48	21
GAIM 3	0.707	44	17
GAIM 3 3-hr	0.672	49	27
GAIM 3 6-hr	0.654	53	34
GAIM 3 12-hr	0.650	57	39
GAIM 3 24-hr	0.649	58	40

measured by the FPMU. The 6, 12, and 24 hour forecasts of GAIM 3 showed slightly stronger correlation than the real time runs of GAIM 2 and GAIM 3, likely due to the real time versions of GAIM "trusting" the assimilated data less than the IFM background because the differences between the two values were deemed too different.

Table 18. Diurnal Run 2 performance of ionospheric model predicted electron density values in relation to FPMU data.

	Day			Night		
Model	**Corr.** (r)	**MAPD** (%)	**MPD** (%)	**Corr.** (r)	**MAPD** (%)	**MPD** (%)
IRI-90	0.647	88	80	0.570	56	43
IRI-12	0.655	44	26	0.549	37	-5
CTIPe	0.565	53	-52	0.528	50	-36
IFM	0.666	56	26	0.519	87	64
GAIM 2	0.720	30	-9	0.548	66	52
GAIM 3	0.724	30	-9	0.567	60	44
GAIM 3 3-hr	0.686	37	6	0.555	62	48
GAIM 3 6-hr	0.675	42	13	0.575	66	55
GAIM 3 12-hr	0.674	44	16	0.581	71	62
GAIM 3 24-hr	0.671	44	18	0.580	73	64

Regionally, all of the models had much lower MAPD values than the overall results at low latitudes (Table 19), largely due to fewer plasma depletions measured by the FPMU at low latitudes during this run. All but the two IRI models showed smaller

positive biases at low latitudes due to fewer plasma depletions there and due to abnormally high FPMU electron density values in the Appleton Anomaly ionization peaks. While both versions of IRI under predicted in the ionization peak areas, they also tended to overestimate the low latitude region in general more than in the overall results, similar to what was seen during Run 1 (also a period of solar minimum).

Table 19. Regional Run 2 performance of ionospheric model predicted electron density values in relation to FPMU data.

Model	Low Latitude ($\|\Lambda\| \leq 30°$)			Mid Latitude ($\|\Lambda\| > 30°$)		
	Corr. (r)	**MAPD** (%)	**MPD** (%)	**Corr.** (r)	**MAPD** (%)	**MPD** (%)
IRI-90	0.610	73	59	0.535	72	63
IRI-12	0.621	49	10	0.512	35	11
CTIPe	0.449	49	-33	0.392	53	-51
IFM	0.586	61	21	0.220	77	59
GAIM 2	0.675	63	37	0.484	39	11
GAIM 3	0.684	57	31	0.517	37	8
GAIM 3 3-hr	0.640	56	29	0.412	45	25
GAIM 3 6-hr	0.621	56	30	0.379	52	36
GAIM 3 12-hr	0.620	58	32	0.373	56	42
GAIM 3 24-hr	0.618	60	35	0.375	57	43

At mid-latitudes, all of the models showed much weaker correlation than in the overall results, likely partially due to the plasma depletions measured there. GAIM 3 performed the best overall, with the second best correlation (0.517) and the second lowest MAPD (39%). IFM performed the worst overall at mid latitudes, with the lowest correlation (0.220) and the highest MAPD (77%). CTIPe tended to underestimate electron densities the most, due to its aforementioned tendency to under predict the plasma depletions. IFM over predicted more at mid than low latitudes because it predicted the mid latitude plasma depletions the worst of all the models during this run.

4.4.2 Electron Temperature.

The overall electron temperature performance of the models during this run was very similar to the overall electron temperature results, with the exception of CTIPe, which showed a significant improvement (Table 20). CTIPe had the best electron temperature performance, with a strong correlation of 0.821 and the lowest electron temperature MAPD value (14%) of any model for any run. IFM again performed the worst, with weak correlation (0.351) and the largest MAPD by a factor of two (41%).

Table 20. Run 2 performance of ionospheric model predicted electron temperature values in relation to FPMU data.

Model	Correlation (r)	MAPD (%)	MPD (%)
IRI-90	0.776	20	-9
IRI-12	0.762	19	-13
CTIPe	0.821	14	0
IFM	0.351	41	-37

All of the models showed slightly worse performance during the day than in the overall results, and poor performance in general (Table 21). The highest correlation (IRI-12) was a weak 0.287, and IFM was nearly completely uncorrelated, with a value of -0.075. However, all of the models tended to perform slightly better at night than for the overall results during these conditions, with IRI-12 again performing the best with the strongest correlation. CTIPe had correlation values of 0.181 and 0.580 during day and night, respectively, but had an overall correlation value much higher than both. This is likely due to outlier data points in both data sets that skewed the correlation for each data set, but had less of an impact on the correlation of all of the data points from the run as a whole. As the number of points in a dataset increases, the effect that outlier data points has on the correlation coefficient diminishes (*Navidi*, 2006).

Regionally, all of the models performed generally well at low latitudes, and all produced better results than in the overall low latitude results (Table 22). CTIPe and

Table 21. Run 2 Diurnal performance of ionospheric model predicted electron temperature values in relation to FPMU data.

Model	Day			Night		
	Corr. (r)	**MAPD** (%)	**MPD** (%)	**Corr.** (r)	**MAPD** (%)	**MPD** (%)
IRI-90	0.212	15	0	0.663	25	-18
IRI-12	0.287	16	-11	0.702	22	-15
CTIPe	0.181	15	1	0.580	12	-1
IFM	-0.075	46	-46	0.304	37	-28

IFM actually had the two strongest correlation values of all the models, with CTIPe performing the best overall. All of the models performed better at mid latitudes except for IFM, which again showed weak correlation at mid latitudes due to the electron temperature model it uses.

Table 22. Run 2 Regional performance of ionospheric model predicted electron temperature values in relation to FPMU data.

Model	Low Latitude ($\|\Lambda\| \leq 30°$)			Mid Latitude ($\|\Lambda\| > 30°$)		
	Corr. (r)	**MAPD** (%)	**MPD** (%)	**Corr.** (r)	**MAPD** (%)	**MPD** (%)
IRI-90	0.721	27	-21	0.739	17	-3
IRI-12	0.697	27	-26	0.737	16	-8
CTIPe	0.776	14	0	0.815	14	-1
IFM	0.754	35	-35	0.212	44	-38

4.5 Run 3 Results - Low Solar Activity and Geomagnetic Storming Conditions

This run occurred during 5-9 April 2010, and featured very low solar activity with geomagnetic storming early in the run period and then gradually decreasing (Figure 15) to quiet conditions.

Average hmF_2, NmF_2, and TEC values for the period are presented in Table 23. Larger average NmF_2 and TEC values are observed during this period due to the increased geomagnetic storming. This is due to an increase in electrons in the

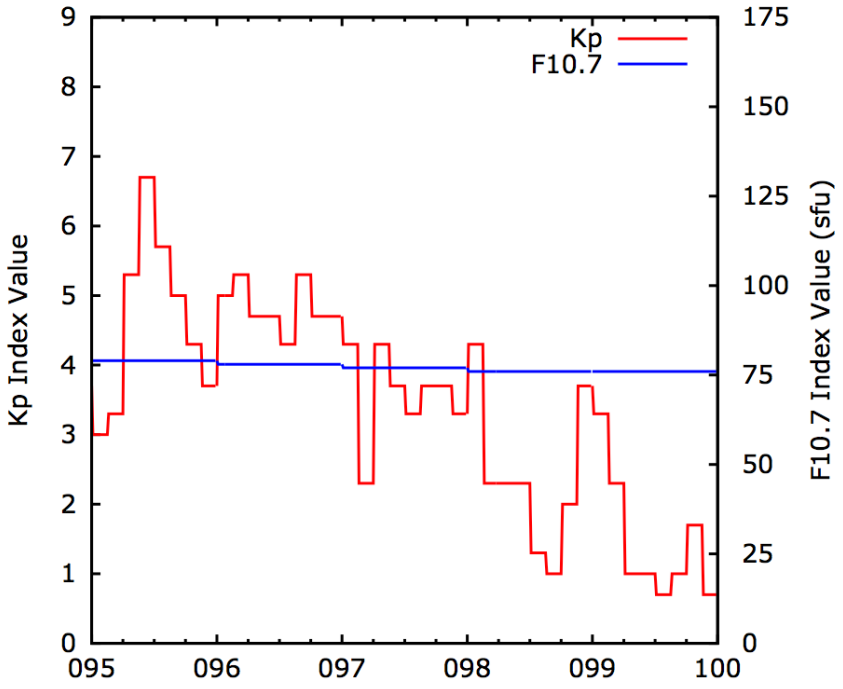

Figure 15. Run 3 Kp and F10.7 Index Values for 5-9 April 2010 ($sfu = 10^{-22} W\ m^{-2}\ s$).

ionosphere coming down from the polar caps (*Schunk and Nagy*, 2009). CTIPe again predicted NmF_2 and TEC values less than half that of the rest of the models, while GAIM 2 and GAIM 3 predicted the largest NmF_2 and IRI-90 predicted the largest TEC. There is also a wider range of hmF_2 values during this run than in the overall results, with the 24 km difference between the lowest predicted hmF_2 (IRI-90) and the largest predicted hmF_2 (CTIPe).

4.5.1 Electron Density.

All of the models produced better results during these moderate geomagnetic storming conditions than the overall set of results, with GAIM 2 and 3 obtaining the highest correlation values (0.941) of any model during any period (Table 24). CTIPe and IFM performed the worst overall, but all of the models showed very good correlation overall. This relative increase in performance suggests the models may

Table 23. Run 3 average model-predicted hmF2, NmF2, and TEC values.

Model	hmF2 (km)	NmF2 (x $10^{11} m^{-3}$)	TEC (x $10^{16} m^{-2}$)
IRI-90	284.45	5.23	15.00
IRI-12	278.48	4.32	12.00
CTIPe	308.61	2.35	5.99
IFM	293.05	5.72	13.44
GAIM 2	286.53	5.75	13.90
GAIM 3	287.02	5.75	13.90
GAIM 3 3-hr	290.21	5.68	13.64
GAIM 3 6-hr	292.30	5.70	13.66
GAIM 3 12-hr	293.01	5.74	13.65
GAIM 3 24-hr	293.04	5.71	13.55

perform better during geomagnetic storming, during periods when the F10.7 index correlates to EUV flux, or both.

Table 24. Run 3 performance of ionospheric model predicted electron density values in relation to FPMU data.

Model	Correlation (r)	MAPD (%)	MPD (%)
IRI-90	0.869	59	27
IRI-12	0.882	41	-12
CTIPe	0.792	61	-56
IFM	0.799	93	49
GAIM 2	0.941	45	14
GAIM 3	0.941	44	14
GAIM 3 3-hr	0.900	59	26
GAIM 3 6-hr	0.892	68	34
GAIM 3 12-hr	0.885	72	38
GAIM 3 24-hr	0.886	72	38

Day time performance during this period was similar to the overall daytime results and very good in terms of correlation (Table 25). At night, all of the models exhibited weaker correlation than in the overall nighttime results. CTIPe performed the worst by far, while GAIM 2 and 3 were the most accurate at night. MPD values were also lower than the overall nighttime results, likely due to fewer plasma depletions measured by the FPMU during this run (based on examining the electron density

plots).

Table 25. Diurnal Run 3 performance of ionospheric model predicted electron density values in relation to FPMU data.

Model	Day			Night		
	Corr. (r)	**MAPD** (%)	**MPD** (%)	**Corr.** (r)	**MAPD** (%)	**MPD** (%)
IRI-90	0.844	60	33	0.438	56	21
IRI-12	0.858	36	-6	0.428	46	-19
CTIPe	0.746	59	-59	0.406	63	-51
IFM	0.756	96	52	0.475	89	45
GAIM 2	0.930	34	0	0.756	58	30
GAIM 3	0.929	35	3	0.764	55	26
GAIM 3 3-hr	0.878	56	22	0.621	64	30
GAIM 3 6-hr	0.871	68	33	0.592	69	35
GAIM 3 12-hr	0.862	72	37	0.572	73	41
GAIM 3 24-hr	0.863	70	34	0.568	73	43

All of the models also exhibited better performance at low latitudes than in the overall results, as well as a general decrease in MPD, again likely due to fewer equatorial plasma bubbles (Table 26). IFM was particularly bad, with a correlation of only 0.242. FPMU encountered some mid-latitude plasma depletions, likely causing this decrease in performance.

Table 26. Regional Run 3 performance of ionospheric model predicted electron density values in relation to FPMU data.

Model	Low Latitude ($\|\Lambda\| \leq 30°$)			Mid Latitude ($\|\Lambda\| > 30°$)		
	Corr. (r)	**MAPD** (%)	**MPD** (%)	**Corr.** (r)	**MAPD** (%)	**MPD** (%)
IRI-90	0.860	51	6	0.564	65	45
IRI-12	0.866	46	-23	0.615	36	-3
CTIPe	0.728	63	-53	0.752	59	-58
IFM	0.815	76	10	0.242	107	82
GAIM 2	0.931	49	17	0.795	42	11
GAIM 3	0.930	46	14	0.789	43	13
GAIM 3 3-hr	0.890	58	14	0.539	60	35
GAIM 3 6-hr	0.887	60	13	0.465	76	53
GAIM 3 12-hr	0.882	62	13	0.426	81	60
GAIM 3 24-hr	0.882	63	15	0.436	80	58

4.5.2 Electron Temperature.

Electron temperature performance during this run was essentially the same as for the overall set of data (Table 27). IRI-90 again was the most accurate, while IFM performed the worst.

Table 27. Run 3 performance of ionospheric model predicted electron temperature values in relation to FPMU data.

Model	Correlation (r)	MAPD (%)	MPD (%)
IRI-90	0.728	24	-23
IRI-12	0.680	30	-29
CTIPe	0.574	22	1
IFM	0.299	48	-46

However, during the daytime both IRI models performed better than the overall daytime results and much better than Runs 1 and 2 (during extreme solar minimum), as seen in Table 28. CTIPe and IFM had worse performance during the day than in the overall results, although even though the overall daytime performance values were already poor. IFM again had a negative correlation value (-0.208), indicating a weak inverse linear relationship. Night performance was very similar to the overall nighttime results, with slightly higher MAPD values and more of a negative bias.

Table 28. Run 3 Diurnal performance of ionospheric model predicted electron temperature values in relation to FPMU data.

	Day			Night		
Model	**Corr.** (r)	**MAPD** (%)	**MPD** (%)	**Corr.** (r)	**MAPD** (%)	**MPD** (%)
IRI-90	0.692	15	-14	0.536	37	-37
IRI-12	0.497	27	-27	0.510	35	-34
CTIPe	0.129	18	10	0.327	27	-9
IFM	-0.208	50	-50	0.353	46	-40

At low-latitudes, all of the models performed similar to the overall low-latitude results, while there was a slight decrease in performance at mid-latitudes, with all models tending to show more of a negative bias than in the overall results (Table 29).

IFM's difficulty in capturing electron temperature trends at mid latitudes is clearly evident in its extremely weak correlation value of 0.093.

Table 29. Run 3 Regional performance of ionospheric model predicted electron temperature values in relation to FPMU data.

Model	Low Latitude ($\|\Lambda\| \leq 30°$)			Mid Latitude ($\|\Lambda\| > 30°$)		
	Corr. (r)	**MAPD** (%)	**MPD** (%)	**Corr.** (r)	**MAPD** (%)	**MPD** (%)
IRI-90	0.674	31	-31	0.518	21	-20
IRI-12	0.671	28	-27	0.420	31	-30
CTIPe	0.551	26	9	0.329	20	-3
IFM	0.656	38	-38	0.093	53	-49

4.6 Run 4 Results - High Solar Activity and Moderate Geomagnetic Storming

Run 4 represented moderate solar and geomagnetic activity and occurred during 1-5 March 2011, with Kp index values peaking at 5+ on day 60 and then decreasing down to 2 by the end of day 64. F10.7 index values steadily increased with each day (Figure 16).

Average hmF_2, NmF_2, and TEC values for the period are presented in Table 30. As expected, elevated NmF_2 and TEC values are predicted during this period compared to the the previous runs due to increased geomagnetic and solar activity. As a result, we also see higher hmF_2 values than in the previous runs, since higher electron densities tend to shift the F_2 peak upward. The same trends within the models held, with CTIPe predicted the smallest NmF_2 and TEC values and IFM predicting the largest NmF_2 and TEC values.

4.6.1 Electron Density.

All of the models except IRI performed worse during this set of conditions than in the overall results (Table 31). Both IRI models showed good performance overall,

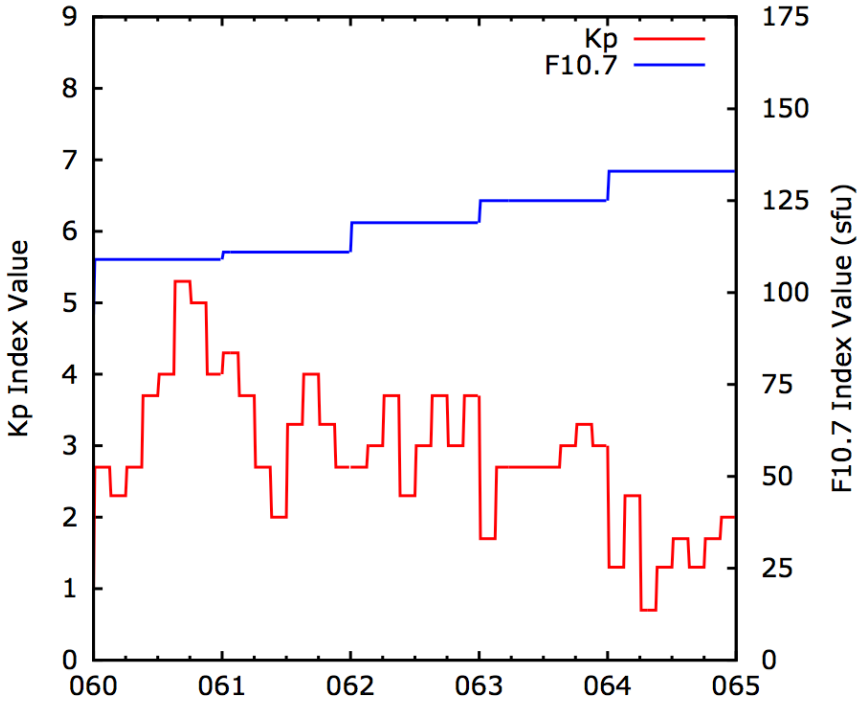

Figure 16. Run 4 Kp and F10.7 Index Values for 1-5 March 2011 ($sfu = 10^{-22} W\ m^{-2}\ s$).

Table 30. Run 4 average model-predicted hmF2, NmF2, and TEC values.

Model	hmF2 (km)	NmF2 (x $10^{11} m^{-3}$)	TEC (x $10^{16} m^{-2}$)
IRI-90	291.99	5.01	14.88
IRI-12	291.97	4.74	13.47
CTIPe	306.12	2.86	8.14
IFM	305.05	7.00	18.80
GAIM 2	301.82	5.54	15.75
GAIM 3	302.10	5.71	15.62
GAIM 3 3-hr	303.11	5.80	16.34
GAIM 3 6-hr	304.15	5.89	16.42
GAIM 3 12-hr	305.22	5.95	16.67
GAIM 3 24-hr	305.08	5.94	16.04

while all of the other models showed relatively weak correlation. IFM and GAIM had very high MAPD and MPD values, with IFM's severe positive bias (two times larger than the overall results) likely causing GAIM's Kalman filter to discard many data assimilation sources due to differences between the background and the data source deemed too large and discarded. IFM's performance issues were likely related to the increase in solar activity across the period, since it didn't seem to struggle with the decreasing geomagnetic activity levels seen in Run 3.

Table 31. Run 4 performance of ionospheric model predicted electron density values in relation to FPMU data.

Model	Correlation (r)	MAPD (%)	MPD (%)
IRI-90	0.845	50	34
IRI-12	0.840	42	21
CTIPe	0.580	53	-25
IFM	0.527	146	128
GAIM 2	0.589	95	73
GAIM 3	0.590	97	76
GAIM 3 3-hr	0.561	107	87
GAIM 3 6-hr	0.541	110	91
GAIM 3 12-hr	0.542	113	95
GAIM 3 24-hr	0.548	110	92

As expected, degraded performance overall was also seen when looking at diurnal trends (Table 32). All of the models tended to overestimate more than in the overall results during the day time. The biggest performance change occurred at night, when IFM and GAIM both overestimated values by at least 121%. Again this is tied to GAIM's reliance on IFM as a background; the greater the differences in IFM background and assimilated data, the less GAIM trusts the data source, leading to a closer relationship between IFM and GAIM performance.

At low-latitudes, both versions of IRI again showed strong performance, while the rest of the models performed worse than in the overall low-latitude results (Table 33). GAIM's reliance on IFM was clearly evident in the performance data, with IFM's

Table 32. Diurnal Run 4 performance of ionospheric model predicted electron density values in relation to FPMU data.

Model	Day			Night		
	Corr. (r)	**MAPD** (%)	**MPD** (%)	**Corr.** (r)	**MAPD** (%)	**MPD** (%)
IRI-90	0.881	52	41	0.620	48	29
IRI-12	0.874	44	28	0.641	40	15
CTIPe	0.610	48	-45	0.516	57	-8
IFM	0.597	96	68	0.484	188	177
GAIM 2	0.680	53	15	0.535	129	121
GAIM 3	0.673	55	18	0.550	132	125
GAIM 3 3-hr	0.641	63	28	0.523	144	135
GAIM 3 6-hr	0.625	66	32	0.510	147	139
GAIM 3 12-hr	0.627	68	36	0.506	151	144
GAIM 3 24-hr	0.635	65	33	0.508	147	140

large MAPD and MPD values in both regions leading to a closer relationship between GAIM and IFM performance. At mid-latitudes, IFM was completely uncorrelated to the FPMU data, leading to extremely weak GAIM correlation values (0.189). All of the models showed worse performance at mid-latitudes than the overall mid-latitude results, tending to overestimate more than in the overall results, likely overcompensating for the increase in the F10 index values, which are generally tied to an increase in electron densities.

4.6.2 Electron Temperature.

Both IRI models performed very similarly during this set of conditions, while CTIPe and IFM showed much worse correlation than in the overall results (Table 34). In fact, IFM was almost completely uncorrelated during the period (0.073).

Day time performance overall was very similar as well; CTIPe and IRI-12 had slightly stronger day time correlation values than the overall results (but still weak overall), while IRI-90 and IFM both had weaker correlation values than the overall results, with IFM again obtaining a negative correlation value (Table 35). At night,

Table 33. Regional Run 4 performance of ionospheric model predicted electron density values in relation to FPMU data.

Model	Low Latitude ($\|\Lambda\| \leq 30°$)			Mid Latitude ($\|\Lambda\| > 30°$)		
	Corr. (r)	**MAPD** (%)	**MPD** (%)	**Corr.** (r)	**MAPD** (%)	**MPD** (%)
IRI-90	0.804	43	17	0.643	55	47
IRI-12	0.795	37	4	0.635	45	32
CTIPe	0.375	61	-9	0.504	47	-36
IFM	0.369	143	113	0.000	148	138
GAIM 2	0.404	113	85	0.189	82	65
GAIM 3	0.405	116	89	0.181	84	67
GAIM 3 3-hr	0.364	126	97	0.180	93	80
GAIM 3 6-hr	0.344	125	94	0.145	100	89
GAIM 3 12-hr	0.348	124	94	0.140	106	96
GAIM 3 24-hr	0.353	122	92	0.153	102	91

Table 34. Run 4 performance of ionospheric model predicted electron temperature values in relation to FPMU data.

Model	Correlation (r)	MAPD (%)	MPD (%)
IRI-90	0.681	32	-30
IRI-12	0.694	25	-22
CTIPe	0.237	35	16
IFM	0.073	41	-36

both IFM and CTIPe were effectively uncorrelated (both with small, negative values). CTIPe also had a much larger positive bias than in the overall results.

Table 35. Run 4 Diurnal performance of ionospheric model predicted electron temperature values in relation to FPMU data.

Model	Day			Night		
	Corr. (r)	**MAPD** (%)	**MPD** (%)	**Corr.** (r)	**MAPD** (%)	**MPD** (%)
IRI-90	0.297	20	-17	0.609	41	-40
IRI-12	0.399	19	-15	0.550	30	-28
CTIPe	0.292	18	-5	-0.054	46	30
IFM	-0.040	50	-48	-0.085	34	-26

Low-latitude performance was worse than the overall results across the board during this period, with CTIPe and IFM almost completely uncorrelated (Table 36). At mid-latitudes, both IRI models performed better than the overall results, while the two physics-based models performed worse, again with IFM data values completely uncorrelated to FPMU values.

Table 36. Run 4 Regional performance of ionospheric model predicted electron temperature values in relation to FPMU data.

Model	Low Latitude ($\|\Lambda\| \leq 30°$)			Mid Latitude ($\|\Lambda\| > 30°$)		
	Corr. (r)	**MAPD** (%)	**MPD** (%)	**Corr.** (r)	**MAPD** (%)	**MPD** (%)
IRI-90	0.448	39	-39	0.650	29	-27
IRI-12	0.491	32	-31	0.657	23	-20
CTIPe	-0.071	46	29	0.234	31	11
IFM	0.020	31	-22	0.050	44	-40

4.7 Run 5 Results - Moderate Solar activity and Moderate Geomagnetic Storming

Run 5 occurred during 30 April - 5 May 2011 and represented moderate solar and geomagnetic activity. Kp index values peaked at 5- on day 120 and decreased

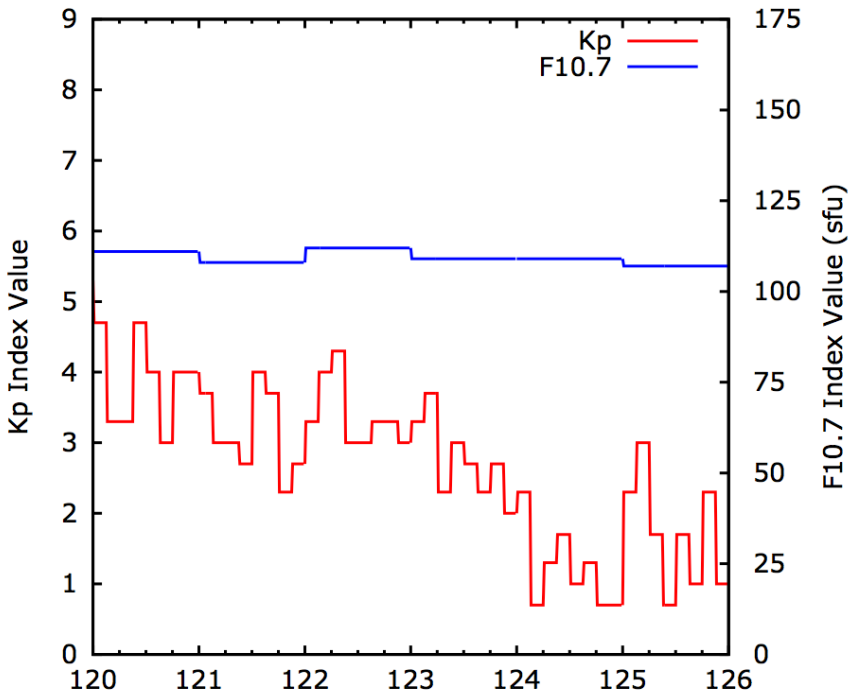

Figure 17. Run 5 Kp and F10.7 Index Values for 30 April - 5 May 2011 ($sfu = 10^{-22} W\ m^{-2}\ s$)**.**

throughout the period, while F10 index values remained relatively constant around 110 (Figure 17).

Average hmF_2, NmF_2, and TEC values for the period are presented in Table 37. Due to the increased solar and geomagnetic activity, hmF_2, NmF_2, and TEC values are all higher in general compared to the overall results and the previous runs. CTIPe again predicted the highest hmF_2, and the lowest NmF_2 and TEC values. IRI-12 predicted the lowest hmF_2, GAIM 2 predicted the largest NmF_2, and GAIM 3 predicted the largest TEC values.

4.7.1 Electron Density.

Model performance during this period was very good overall, and better than the overall results with the exception of CTIPe (Table 38). All of the GAIM forecasts also performed better than both IRI models and CTIPe during the period, likely due to

Table 37. Run 5 average model-predicted hmF2, NmF2, and TEC values.

Model	hmF2 (km)	NmF2 (x $10^{11} m^{-3}$)	TEC (x $10^{16} m^{-2}$)
IRI-90	299.77	5.89	18.16
IRI-12	294.57	5.29	15.54
CTIPe	308.41	3.10	9.23
IFM	304.70	6.67	17.05
GAIM 2	303.99	7.15	19.09
GAIM 3	304.39	6.99	19.16
GAIM 3 3-hr	305.56	7.00	18.72
GAIM 3 6-hr	306.43	7.06	18.66
GAIM 3 12-hr	306.86	7.08	18.57
GAIM 3 24-hr	306.79	7.08	18.78

IFM's improved performance. CTIPe had weaker correlation than the overall results, and tended to underestimate electron densities more during this period.

Table 38. Run 5 performance of ionospheric model predicted electron density values in relation to FPMU data.

Model	Correlation (r)	MAPD (%)	MPD (%)
IRI-90	0.850	56	19
IRI-12	0.841	47	-2
CTIPe	0.686	57	-46
IFM	0.790	66	25
GAIM 2	0.912	46	18
GAIM 3	0.914	45	16
GAIM 3 3-hr	0.883	53	23
GAIM 3 6-hr	0.879	56	27
GAIM 3 12-hr	0.877	57	29
GAIM 3 24-hr	0.879	58	30

During the day, all of models except CTIPe also performed better than the overall daytime results (Table 39). GAIM 2 and 3 had very strong correlation to FPMU values, and all of the models except CTIPe showed very little overall bias. Again the effect of IFM's improved performance was clearly evident in the GAIM models, with all of the GAIM runs exhibiting very strong correlation. Night time performance during this period was slightly better than overall night performance. All of the

models also displayed a decrease in MPD values across the board.

Table 39. Diurnal Run 5 performance of ionospheric model predicted electron density values in relation to FPMU data.

Model	Day			Night		
	Corr. (r)	**MAPD** (%)	**MPD** (%)	**Corr.** (r)	**MAPD** (%)	**MPD** (%)
IRI-90	0.890	44	10	0.761	67	28
IRI-12	0.893	37	-8	0.761	57	4
CTIPe	0.696	53	-50	0.602	61	-43
IFM	0.849	46	4	0.663	86	44
GAIM 2	0.935	29	-3	0.850	63	39
GAIM 3	0.936	29	-3	0.853	60	36
GAIM 3 3-hr	0.915	37	5	0.791	69	41
GAIM 3 6-hr	0.915	39	8	0.779	73	46
GAIM 3 12-hr	0.913	40	9	0.781	74	49
GAIM 3 24-hr	0.914	41	10	0.782	74	49

Regionally, CTIPe performed worse than the overall results at low latitudes (Table 40), tending to severely under predicting equatorial electron densities at night. All of the other models showed a decrease in MPD values as well, also due to under predicting the high electron densities experienced by the FPMU at night near the equator. Mid latitude performance was slightly better than the overall results across the board.

4.7.2 Electron Temperature.

Overall electron temperature performance during this period was slightly worse than the overall results, but mainly only in the form of weaker correlation values (Table 41). During the day, CTIPe performed significantly worse than the overall daytime results, obtaining a negative correlation value (Table 42). At night, all of the models underestimated more than in the overall night time results and tended to under predict electron temperatures more. While low-latitude performance was mostly similar to the overall results, all of the models performed worse than the

Table 40. Regional Run 5 performance of ionospheric model predicted electron density values in relation to FPMU data.

Model	Low Latitude ($\|\Lambda\| \leq 30°$)			Mid Latitude ($\|\Lambda\| > 30°$)		
	Corr. (r)	**MAPD** (%)	**MPD** (%)	**Corr.** (r)	**MAPD** (%)	**MPD** (%)
IRI-90	0.778	65	19	0.833	49	20
IRI-12	0.771	57	-1	0.833	40	-2
CTIPe	0.527	61	-40	0.734	53	-51
IFM	0.719	73	13	0.720	61	34
GAIM 2	0.866	57	26	0.923	38	12
GAIM 3	0.870	55	25	0.925	37	10
GAIM 3 3-hr	0.833	60	26	0.853	47	21
GAIM 3 6-hr	0.830	62	27	0.837	51	28
GAIM 3 12-hr	0.828	63	27	0.835	53	31
GAIM 3 24-hr	0.830	63	27	0.836	53	31

overall results at mid-latitudes, especially IFM (Table 43). IFM tended to under predict electron temperatures more than in the overall results at mid-latitudes, in spite of the fact it severely over predicted electron temperatures (sometimes by over 2000 K) on several occasions at night around $-50°$ latitude.

Table 41. Run 5 performance of ionospheric model predicted electron temperature values in relation to FPMU data.

Model	Correlation (r)	MAPD (%)	MPD (%)
IRI-90	0.665	27	-26
IRI-12	0.684	25	-24
CTIPe	0.481	27	0
IFM	0.284	44	-43

4.8 Run 6 Results - High Solar Activity and Low Geomagnetic Activity

Run 6 occurred during 19-23 October 2011 and represented high solar activity (peaking at a F10.7 value of 164 on day 294) and a Kp index value of 2+ (Figure 18).

Average hmF_2, NmF_2, and TEC values for the period are presented in Table 44, and show some distinct differences in relation to the overall averages. The effect of increased solar activity on electron densities is clearly evident, with the highest

Table 42. Run 5 Diurnal performance of ionospheric model predicted electron temperature values in relation to FPMU data.

Model	Day			Night		
	Corr. (r)	MAPD (%)	MPD (%)	Corr. (r)	MAPD (%)	MPD (%)
IRI-90	0.349	17	-13	0.492	37	-37
IRI-12	0.334	15	-13	0.508	34	-33
CTIPe	-0.321	25	8	0.158	27	-6
IFM	0.058	48	-48	0.100	40	-38

Table 43. Run 5 Regional performance of ionospheric model predicted electron temperature values in relation to FPMU data.

Model	Low Latitude ($\|\Lambda\| \leq 30°$)			Mid Latitude ($\|\Lambda\| > 30°$)		
	Corr. (r)	MAPD (%)	MPD (%)	Corr. (r)	MAPD (%)	MPD (%)
IRI-90	0.691	35	-35	0.481	25	-22
IRI-12	0.693	31	-30	0.490	22	-21
CTIPe	0.424	24	6	0.281	28	-3
IFM	0.613	33	-33	0.091	49	-46

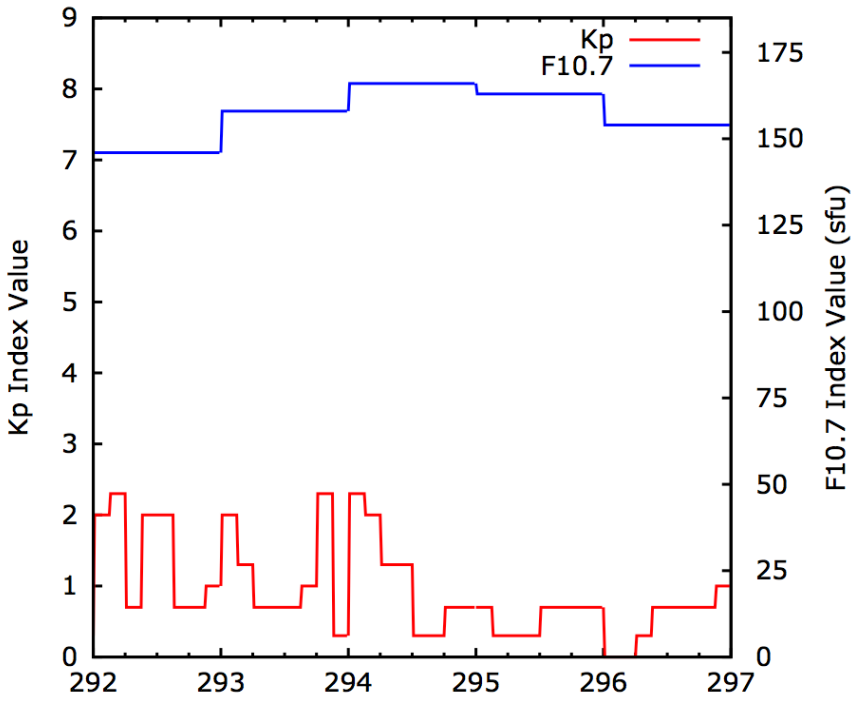

Figure 18. Run 6 Kp and F10.7 Index Values for 19-23 October 2011 ($sfu = 10^{-22} W\ m^{-2}\ s$).

average values calculated during this run. The largest difference (30.5 km) in between the lowest (IRI-12) and highest (CTIPe) hmF_2 values was also observed. Otherwise the same general trends seen in the overall results hold during this run. CTIPe again predicted NmF_2 and TEC values nearly half that of the others, and IFM predicted the largest TEC values.

Table 44. Run 6 average model-predicted hmF2, NmF2, and TEC values.

Model	**hmF2** (km)	**NmF2** (x $10^{11} m^{-3}$)	**TEC** (x $10^{16} m^{-2}$)
IRI-90	305.56	6.91	21.66
IRI-12	300.13	7.13	21.42
CTIPe	330.60	4.67	15.64
IFM	326.58	10.73	32.46
GAIM 2	323.52	9.15	29.41
GAIM 3	323.79	9.34	29.41
GAIM 3 3-hr	325.74	9.65	30.02
GAIM 3 6-hr	327.10	9.89	30.60
GAIM 3 12-hr	327.26	9.96	30.86
GAIM 3 24-hr	327.23	9.95	30.87

4.8.1 Electron Density.

Electron density results for this run were better than the overall results and very good in general, suggesting the models can account for increased geomagnetic or solar activity, but not both at the same time (Table 45). All of the models tended to have a smaller positive or more negative bias during this period; CTIPe and both IRI models exhibited an overall negative bias, while IFM and the GAIM models had a positive bias.

Daytime performance during this period was better across the board, although all of the models tended to under predict more than in the overall results during the day, with all but IFM exhibiting a negative bias (Table 46). Correlation weakened more at night than in the overall results, but MAPD values decreased across the

Table 45. Run 6 performance of ionospheric model predicted electron density values in relation to FPMU data.

Model	Correlation (r)	MAPD (%)	MPD (%)
IRI-90	0.903	38	-17
IRI-12	0.896	39	-24
CTIPe	0.810	58	-47
IFM	0.811	68	41
GAIM 2	0.919	40	7
GAIM 3	0.916	40	8
GAIM 3 3-hr	0.901	48	18
GAIM 3 6-hr	0.893	51	24
GAIM 3 12-hr	0.893	52	26
GAIM 3 24-hr	0.893	52	27

board as well, with lower MPD values for all models. As seen in the overall results for this period, performance at low and mid latitudes was better than the overall low and mid latitude results, and all models again showed lower bias values than in the overall results (Table 47).

Table 46. Diurnal Run 6 performance of ionospheric model predicted electron density values in relation to FPMU data.

Model	Day			Night		
	Corr. (r)	**MAPD** (%)	**MPD** (%)	**Corr.** (r)	**MAPD** (%)	**MPD** (%)
IRI-90	0.878	37	-29	0.561	40	-3
IRI-12	0.864	40	-33	0.605	38	-14
CTIPe	0.800	60	-60	0.347	56	-33
IFM	0.797	47	9	0.622	92	78
GAIM 2	0.910	27	-16	0.676	55	33
GAIM 3	0.904	27	-15	0.674	56	34
GAIM 3 3-hr	0.887	31	-7	0.633	66	47
GAIM 3 6-hr	0.876	34	-3	0.641	70	55
GAIM 3 12-hr	0.880	33	-3	0.637	74	59
GAIM 3 24-hr	0.881	33	-3	0.636	74	60

Table 47. Regional Run 6 performance of ionospheric model predicted electron density values in relation to FPMU data.

Model	Low Latitude ($\|\Lambda\| \leq 30°$)			Mid Latitude ($\|\Lambda\| > 30°$)		
	Corr. (r)	**MAPD** (%)	**MPD** (%)	**Corr.** (r)	**MAPD** (%)	**MPD** (%)
IRI-90	0.880	45	-21	0.800	34	-14
IRI-12	0.876	45	-29	0.779	34	-20
CTIPe	0.764	56	-33	0.686	59	-57
IFM	0.755	84	52	0.613	57	34
GAIM 2	0.890	47	13	0.880	35	2
GAIM 3	0.885	47	14	0.879	36	3
GAIM 3 3-hr	0.872	56	25	0.809	41	14
GAIM 3 6-hr	0.862	60	31	0.788	44	19
GAIM 3 12-hr	0.862	63	34	0.795	45	21
GAIM 3 24-hr	0.861	63	34	0.799	45	21

4.8.2 Electron Temperature.

Electron temperature correlation improved in all models during this run; all but IFM showed strong correlation, and CTIPe had the strongest correlation of all models (Table 48). All of the models had higher MPD values than in the overall results as well, which is likely related to the overall decrease in electron density MPD values. Day time correlation improved for all but IFM, which again was effectively uncorrelated during the daytime. Night time performance was better than than the overall results across the board (Table 49). The same general trends seen in the overall run performance were also seen in the regional breakdown (Table 50).

Table 48. Run 6 performance of ionospheric model predicted electron temperature values in relation to FPMU data.

Model	Correlation (r)	MAPD (%)	MPD (%)
IRI-90	0.806	22	-18
IRI-12	0.816	15	-8
CTIPe	0.824	31	30
IFM	0.619	27	-27

Table 49. Run 6 Diurnal performance of ionospheric model predicted electron temperature values in relation to FPMU data.

Model	Day			Night		
	Corr. (r)	**MAPD** (%)	**MPD** (%)	**Corr.** (r)	**MAPD** (%)	**MPD** (%)
IRI-90	0.644	16	-12	0.561	25	-20
IRI-12	0.456	14	-7	0.753	16	-9
CTIPe	0.452	40	39	0.851	27	27
IFM	-0.017	39	-39	0.534	22	-22

Table 50. Run 6 Regional performance of ionospheric model predicted electron temperature values in relation to FPMU data.

Model	Low Latitude ($\|\Lambda\| \leq 30°$)			Mid Latitude ($\|\Lambda\| > 30°$)		
	Corr. (r)	**MAPD** (%)	**MPD** (%)	**Corr.** (r)	**MAPD** (%)	**MPD** (%)
IRI-90	0.887	31	-31	0.779	18	-12
IRI-12	0.798	21	-18	0.808	13	-4
CTIPe	0.703	34	34	0.909	28	27
IFM	0.750	20	-20	0.616	30	-30

V. Conclusions and Recommendations

5.1 Chapter Overview

This chapter consists of two main sections. First, a summary will be provided of the results of comparing FPMU electron densities to various ionospheric models, to include recommendations of models for NASA mission planning use. Then, recommendations for future FPMU and model validation efforts will be presented.

5.2 Conclusions

GAIM and IRI-12 most accurately modeled the ISS plasma environment for the dates considered in this effort. GAIM modeled the electron density trends the best, while IRI-12 produced the lowest average errors and the smallest overall bias. GAIM performed very well at predicting electron density values due to its data assimilation scheme. This was especially impressive considering GAIM's 3-D output was the coarsest of all of the models. The addition of the DMSP data source didn't significantly shift the F_2 peak or have a significant effect on performance for ISS orbits, likely due to the altitudes considered in this effort. GAIM's reliance on IFM background values likely significantly impacted its performance during periods when IFM had the largest errors (during deep solar minimum and periods of simultaneous moderate solar and geomagnetic activity). As IFM's errors grow, the impact of GAIM's assimilated data diminishes, since assimilated data values that produce differences relative to the IFM background that are larger than the uncertainty associated with that data are discarded or have a weak weighting applied to them. The two physics based models performed the worst overall, most often obtaining the weakest correlation coefficient values and highest error and biases. IRI-12's improvements over IRI-90 were clearly evident, with an 18% decrease in MAPD values, likely due to many more years worth

of averaged data and improved NmF_2 and topside electron density models. Average errors were relatively high overall (greater than 46%). While these high average errors confirm the importance of performing a validation effort at this altitude, some of these errors could be due to FPMU measurement errors since a robust validation effort and error analysis has not been performed to date for the FPMU.

These trends carried over to electron temperature values. IFM's mid-latitude electron temperature model performed extremely poorly. The performance of both IRI models overall was very impressive across both electron densities and electron temperatures.

From an ISS mission planning standpoint, GAIM and IRI-12 represent the best options for predicting ISS electron densities. Additionally, even if GAIM's performance is skewed significantly by its IFM background, IFM's tendency to overestimate values across all conditions actually provides more of a worst-case set of charging conditions, since high-density, cold plasma produces the largest amount of ISS charging in general. IFM's large negative electron temperature bias adds to this effect. Conversely, CTIPe's tendency to underestimate electron densities and overestimate electron temperatures indicates it would not be a good candidate for ISS mission planning, since it would likely under predict the magnitude of ISS charging. IRI-12's strong performance across both electron densities and temperatures (overall and during the daytime) and its tendency to slightly overestimate electron densities and underestimate electron temperatures indicate it would also be a good solution for ISS mission planning. Additionally, IRI-12 is much more computationally efficient, since no interpolation would have to take place to produce ISS predicted values, and GAIM also requires IFM output to run. Overall, IRI-12 currently represents the best choice as a NASA real-time mission planning tool.

5.3 Recommendations for Future Work

There are many opportunities for future work that complements this effort, both from a model validation standpoint and for providing NASA with a better ionospheric model than what is currently in use for mission planning.

One potential area of follow-on research is the investigation of creating an "ensemble" model for predicting ISS electron density values comprised of some of the models used in this effort, with weights driven by solar and geomagnetic activity levels. With the relatively strong correlation coefficient values that some of the models showed, ensemble modeling that attempts to correct for some of the biases and errors based on geomagnetic and solar activity could provide for more accurate ISS ionospheric predictions.

A more detailed understanding of geomagnetic and solar activity effects on performance can be obtained by examining a larger number of days for each set of conditions. This would reduce the effect outlier data points have on the analysis, and provide a better idea of "normal" performance for each set of conditions. It could also be useful to examine the space weather events leading to increased geomagnetic storming levels (as measured by the Kp index) to analyze how well the Kp index acts as a proxy in the ionospheric models for those events.

Lastly, to build on the results of this effort, a similar study could be performed using the US Air Force Academy's Integrated Miniaturized ElectroStatic Analyzer (iMESA) device aboard the ISS, which also measures electron densities and electron temperatures. This could help further validate the results presented here.

Appendix A. IRI Inputs

1.1 IRI-90

These are the input flags that were used for running IRI-90:

```
T          JF(1)=.TRUE.[.FALSE.]   ELECTRON DENSITY IS [NOT] CALCULATED
T          JF(2)=T[F]    TEMPERATURES ARE [NOT] CALCULATED
T          JF(3)=T[F]    ION COMPOSITION IS [NOT] CALCULATED
T          JF(4)=T[F]    B0 FROM TABLE [FROM GULYEAVA 1987]
F          JF(5)=T[F]    F2 PEAK FROM CCIR [FROM URSI]
T          JF(6)=T[F]    ION COMP. STANDARD [DANILOV-YAICHNIKOV-1985]
T          JF(7)=T[F]    STAND. IRI TOPSIDE [IRI-79]
T          JF(8)=T[F]    NMF2 PEAK MODEL [INPUT VALUES]
T          JF(9)=T[F]    HMF2 PEAK MODEL [INPUT VALUES]
T          JF(10)=T[F]   TE MODEL [TE-NE MODEL WITH NE INPUT]
T          JF(11)=T[F]   NE STANDARD [LAY-FUNCTIONS VERSION]
F          JF(12)=T[F]   MESSAGE ARE WRITTEN TO UNIT=12 [=6]
```

1.2 IRI-12

These are the input flags that were used for running IRI-12:

```
i       .true.                  .false.          standard version
-------------------------------------------------------------------
1    Ne computed            Ne not computed                    T
2    Te, Ti computed        Te, Ti not computed                T
3    Ne & Ni computed       Ni not computed                    T
4    B0 - Table option      B0 - other models jf(31)           T
```

```
 5    foF2 - CCIR            foF2 - URSI                          F
 6    Ni - DS-95 & DY-85     Ni - RBV-10 & TTS-03                 T
 7    Ne - Tops: f10.7<188   f10.7 unlimited                      T
 8    foF2 from model        foF2 or NmF2 - user input            T
 9    hmF2 from model        hmF2 or M3000F2 - user input         T
10    Te - Standard          Te - Using Te/Ne correlation         T
11    Ne - Standard Profile  Ne - Lay-function formalism          T
12    Messages to unit 6     to meesages.text on unit 11          F
13    foF1 from model        foF1 or NmF1 - user input            T
14    hmF1 from model        hmF1 - user input (only Lay version)t
15    foE  from model        foE or NmE - user input              T
16    hmE  from model        hmE - user input                     T
17    Rz12 from file         Rz12 - user input                    T
18    IGRF dip, magbr, modip old FIELDG using POGO68/10 for 1973 t
19    F1 probability model   critical solar zenith angle (old)    T
20    standard F1            standard F1 plus L condition         T
21    ion drift computed     ion drift not computed               F
22    ion densities in \%     ion densities in m-3                 T
23    Te_tops (Aeros,ISIS)   Te_topside (TBT-2011)                F
24    D-region: IRI-95       Special: 3 D-region models           T
25    F107D from APF107.DAT  F107D user input (oarr(41))          T
26    foF2 storm model       no storm updating                    T
27    IG12 from file         IG12 - user                          T
28    spread-F probability   not computed                    F
29    IRI01-topside          new options as def. by JF(30)        F
30    IRI01-topside corr.    NeQuick topside model     false   F
```

```
(29,30) = (t,t) IRIold, (f,t) IRIcor, (f,f) NeQuick, (t,f) Gulyaeva
  31    B0,B1 ABT-2009    B0 Gulyaeva h0.5                    T
  32    F10.7_81 from file     PF10.7_81 - user input (oarr(46))   T
  33    Auroral boundary model on/off  true/false                T
  34    Messages on            Messages off                        F
  35    foE storm model        no foE storm updating               T
```

Bibliography

Aubury, M., and W. Luk (1995), Binomial filters, *Journal of VLSI Signal Processing*, *i*(1-8).

Banks, P. M., R. W. Schunk, and W. J. Raitt (1976), The topside ionosphere: A region of dynamic transition, *Annual Review of Earth and Planetary Sciences*, *4*(1), 381–440, doi:10.1146/annurev.ea.04.050176.002121.

Barjatya, A., C. M. Swenson, D. C. Thompson, and K. H. Wright (2009), Data analysis of the floating potential measurement unit aboard the international space station, *Review of Scientific Instruments*, *80*(4), 041,301–041,311, m3: Article.

Bilitza, D., and B. W. Reinisch (2008), International reference ionosphere 2007: Improvements and new parameters, *Advances in Space Research*, *42*(4), 599–609.

Bilitza, D., L.-A. McKinnell, B. Reinisch, and T. Fuller-Rowell (2011), The international reference ionosphere today and in the future, *Journal of Geodesy*, *85*(12), 909–920, j2: J Geod.

Carruth, M. R., T. Schneider, M. McCollum, M. Finckenor, R. Suggs, D. Ferguson, I. Katz, R. Mikatarian, J. Alred, and C. Pankop (2001), Iss and space environment interactions in event of plasma contactor failure, *Spacecraft Charging Technology Conference Proceedings*, *7th*, 95.

Chen, Y., L. Liu, and W. Wan (2011), Does the f10.7 index correctly describe solar euv flux during the deep solar minimum of 2007-2009?, *Journal of Geophysical Research: Space Physics*, *116*(A4), – A04,304.

Codrescu, M. V., C. Negrea, M. Fedrizzi, T. Fuller-Rowell, A. Dobin, N. Jakowsky, H. Khalsa, T. Matsuo, and N. Maruyama (2012), A real-time run of the coupled thermosphere ionosphere plasmasphere electrodynamics (ctipe) model, *SPACE WEATHER-THE INTERNATIONAL JOURNAL OF RESEARCH AND APPLICATIONS*, *10*.

Coffey, V. N., K. H. Wright, J. I. Minow, T. A. Schneider, J. A. Vaughn, P. D. Craven, M. O. Chandler, S. L. Koontz, L. N. Parker, and T. H. Bui (2008), Validation of the plasma densities and temperatures from the iss floating potential measurement unit, *Plasma Science, IEEE Transactions on*, *36*(5), 2301–2308, iD: 1.

Emmert, J. T., J. L. Lean, and J. M. Picone (2010), Record-low thermospheric density during the 2008 solar minimum, *Geophysical Research Letters*, *37*(12), – L12,102.

Ferguson, D. C. (2009), Fpp results - final report, *Plasma Science, IEEE Transactions on*, *37*(2), 369–374.

Ferguson, D. C., R. Personen, T. L. Morton, and G. B. Hillard (2003), Iss fpp ionospheric electron density and temperature measurements - results, comparison with the iri-90 model, and implications for iss charging.

Gurgew, D. (2011), Modeling ionosphere environments: Creating an iss electron density tool, *Internship final report*, NASA Marshall Space Flight Center.

Huang, C. Y., F. A. Marcos, P. A. Roddy, M. R. Hairston, W. R. Coley, C. Roth, S. Bruinsma, and D. E. Hunton (2009), Broad plasma decreases in the equatorial ionosphere, *Geophysical Research Letters*, *36*(18), – L00C04.

Minow, J. (2012), National Aeronautics and Space Administration Marshall Space Flight Center, Huntsville, AL, Personal Correspondence.

Minow, J. I., L. F. Neergaard, T. H. Bui, R. Mikatarian, H. Barsamian, and S. L. Koontz (2002), Specification of the iss plasma environment variability, in *8th Spacecraft Charging Technology Conference, 20-24 Oct 2003*.

Navidi, W. (2006), *7.1 Correlation*, pp. 475–492, Statistics for Engineers and Scientists, first ed., McGraw HIll, New York, NY.

Reinisch, B. W., and X. Huang (2001), Deducing topside profiles and total electron content from bottomside ionograms, *Advances in Space Research*, *27*(1), 23–30.

Scherliess, L., R. W. Schunk, J. J. Sojka, D. C. Thompson, and L. Zhu (2006), Utah state university global assimilation of ionospheric measurements gauss-markov kalman filter model of the ionosphere: Model description and validation, *Journal Of Geophysical Research-Space Physics*, *111*.

Schunk, R. (2012), Utah State University, Logan UT, Personal Correspondence.

Schunk, R. W., and A. Nagy (2009), *Ionospheres: Physics, Plasma Physics, and Chemistry*, second ed., Cambridge University Press, Cambridge, UK.

Schunk, R. W., J. J. Sojka, and M. D. Bowline (1986), Theoretical study of the electron temperature in the high-latitude ionosphere for solar maximum and winter conditions, *Journal of Geophysical Research: Space Physics*, *91*(A11), 12,041–12,054.

Steadman, L. H. (2011), Effects of storm enhanced densities on geo-location accuracy over conus, M. S. thesis, Air Force Institute of Technology, Wright-Patterson AFB.

Tascione, T. (2010), *Introduction to the Space Environment*, 2nd ed., Krieger Publishing, Malabar, Florida.

Titheridge, J. E. (1998), Temperatures in the upper ionosphere and plasmasphere, *Journal of Geophysical Research: Space Physics*, *103*(A2), 2261–2277.

Wright, K. H., C. M. Swenson, D. C. Thompson, A. Barjatya, S. L. Koontz, T. A. Schneider, J. A. Vaughn, J. I. Minow, P. D. Craven, V. N. Coffey, L. N. Parker, and T. H. Bui (2008), Charging of the international space station as observed by the floating potential measurement unit: Initial results, *Plasma Science, IEEE Transactions on*, *36*(5), 2280–2293, iD: 2.

Zhu, L., R. W. Schunk, G. Jee, L. Scherliess, J. J. Sojka, and D. C. Thompson (2006), Validation study of the ionosphere forecast model using the topex total electron content measurements, *Radio Sci*, *41*(RS5S11).

Vita

Captain David Broadwater was born in Merced, California. After graduating from Golden Valley High School in 2003 as a valedictorian, he studied physics at Loyola Marymount University. He graduated with honors with a Bachelor of Science degree in physics in May 2007. In June 2007 he commissioned into the United States Air Force through the Reserve Officer Training Corps, Detachment 040, at Loyola Marymount University.

Captain Broadwater's first assignment was to the Directed Energy Bioeffects Division in AFRL's Human Effectiveness Directorate at Brooks City-Base, TX as a laser safety scientist. In September 2011, he entered the Graduate Applied Physics program, School of Engineering, Air Force Institute of Technology to obtain a Master's Degree in applied physics with a specialization in space physics. Upon graduation, Captain Broadwater will be assigned to the Persistent Infrared Squadron at the National Air and Space Intelligence Center (NASIC) at Wright-Patterson AFB, OH.

REPORT DOCUMENTATION PAGE

Form Approved
OMB No. 0704–0188

1. REPORT DATE *(DD–MM–YYYY)*	2. REPORT TYPE	3. DATES COVERED *(From — To)*
21–03–2013	Master's Thesis	Sept 2011 — Mar 2013

4. TITLE AND SUBTITLE

A Comparison of Ionospheric Model Performance for International Space Station Orbits

5a. CONTRACT NUMBER

5b. GRANT NUMBER

5c. PROGRAM ELEMENT NUMBER

6. AUTHOR(S)

Broadwater, David J., Captain, USAF

5d. PROJECT NUMBER

5e. TASK NUMBER

5f. WORK UNIT NUMBER

7. PERFORMING ORGANIZATION NAME(S) AND ADDRESS(ES)

Air Force Institute of Technology
Graduate School of Engineering and Management (AFIT/EN)
2950 Hobson Way
WPAFB OH 45433-7765

8. PERFORMING ORGANIZATION REPORT NUMBER

AFIT-ENP-13-M-04

9. SPONSORING / MONITORING AGENCY NAME(S) AND ADDRESS(ES)

Lt Col Robb Randall	Dr. Robert Schunk	Dr. Joseph Minow
Air Force Weather Agency	Utah State Univ. - CASS	NASA - MSFC
101 Nelson Drive	4405 Old Main Hill, Rm 246	Code EV44
Offutt AFB, NE 68113	Logan, UT 84322	Huntsville, AL 35812
402-294-9747	435-797-2961	256-544-2850
robb.randall@offutt.af.mil	shawna@cc.usu.edu	joseph.minow@nasa.gov

10. SPONSOR/MONITOR'S ACRONYM(S)

AFWA, NASA/MSFC, USU CASS

11. SPONSOR/MONITOR'S REPORT NUMBER(S)

12. DISTRIBUTION / AVAILABILITY STATEMENT

DISTRIBUTION STATEMENT A.
APPROVED FOR PUBLIC RELEASE; DISTRIBUTION UNLIMITED.

13. SUPPLEMENTARY NOTES

14. ABSTRACT

The Floating Potential Measurement Unit (FPMU) aboard the International Space Station (ISS) monitors the ISS charging environment and provides a unique electron density and electron temperature in-situ data source for the purpose of ionospheric model validation. An ionospheric model that accurately predicts the ISS plasma environment is desirable for ISS mission planning and situational awareness when FPMU data is unavailable. Electron densities and temperatures from four ionospheric models (International Reference Ionosphere [IRI], Coupled Thermosphere Ionosphere Plasmasphere Electrodynamics model [CTIPe], Ionospheric Forecast Model [IFM], and Global Assimilation of Ionospheric Measurements model [GAIM]) were compared to in-situ FPMU values across a range of geomagnetic and solar conditions. The climatological and assimilative models (IRI and GAIM) performed the best overall across all conditions, while the pure physics based models (IFM and CTIPe) struggled the most to accurately predict the ISS plasma environment. IRI-2012 and GAIM represent the best candidates for use by NASA as an ISS mission planning tool.

15. SUBJECT TERMS

Ionosphere, Ionospheric Model, IRI, CTIPe, IFM, GAIM, ISS, FPMU, Electron Density, Electron Temperature

16. SECURITY CLASSIFICATION OF:			17. LIMITATION OF ABSTRACT	18. NUMBER OF PAGES	19a. NAME OF RESPONSIBLE PERSON
a. REPORT	b. ABSTRACT	c. THIS PAGE			Lt Col Ariel O. Acebal
U	U	U	UU	104	19b. TELEPHONE NUMBER *(include area code)* (937) 255-3636, x4518; ariel.acebal@afit.edu